

## **Preservation of stemness in high-grade serous ovarian cancer organoids requires low Wnt environment**

Karen Hoffmann<sup>1,6</sup>, Hilmar Berger<sup>1</sup>, Hagen Kulbe<sup>2</sup>, Sukanya Thillainadarasan<sup>1</sup>, Hans-Joachim Mollenkopf<sup>1</sup>, Tomasz Zemojtel<sup>3</sup>, Eliane Taube<sup>4</sup>, Silvia Darb-Esfahani<sup>4</sup>, Mandy Mangler<sup>5</sup>, Jalid Sehouli<sup>2</sup>, Radoslav Chekerov<sup>2</sup>, Elena Braicu<sup>2</sup>, Thomas F. Meyer<sup>1,\*</sup> and Mirjana Kessler<sup>1,6,\*</sup>

<sup>1</sup> Department of Molecular Biology, Max Planck Institute for Infection Biology, Berlin, Germany

<sup>2</sup> Department of Gynecology, Charité University Medicine, Campus Virchow-Klinikum, Berlin, Germany

<sup>3</sup> BIH Genomics Core Unit, Charité University Medicine, Campus Virchow-Klinikum, Berlin, Germany

<sup>4</sup> Department of Pathology, Charité University Medicine, Campus Charité, Berlin, Germany

<sup>6</sup> Present address: Department of Internal Medicine/Infectious Diseases and Pulmonary Medicine, Charité University Medicine

### Corresponding authors:

Prof. Thomas F. Meyer, [tfm@mpiib-berlin.mpg.de](mailto:tfm@mpiib-berlin.mpg.de)

Dr. Mirjana Kessler, [mirjana.kessler@charite.de](mailto:mirjana.kessler@charite.de)

## **Running title: Wnt inhibits HGSOC stemness**

26 **Summary**

27 High-grade serous ovarian cancer (HGSOC) likely originates from the fallopian tube (FT) epithelium.  
28 Here, we established 15 organoid lines from HGSOC primary tumor deposits that closely match the  
29 parental tumor mutational profile and phenotype. We found that Wnt pathway activation leads to  
30 growth arrest of these cancer organoids. Moreover, active BMP signaling is almost always required for  
31 generation of HGSOC organoids, while healthy FT organoids depend on BMP suppression by Noggin.  
32 Interestingly, FT organoids modified by stable shRNA knockdown (KD) of p53, PTEN, and  
33 Retinoblastoma (RB), also require a low Wnt environment for long-term growth, while FT organoid  
34 medium triggers growth arrest. Thus, early changes in the stem cell niche environment are needed to  
35 support outgrowth of these genetically altered cells. Indeed, comparative analysis of gene expression  
36 pattern and phenotype of normal and KD organoids confirmed that depletion of tumor suppressors  
37 triggers changes in the regulation of stemness and differentiation.

38

39 **Keywords:** organoids, p53, PTEN, Retinoblastoma, BMP signaling

40 **Introduction**

41 High-grade serous ovarian cancer (HGSOC), an occult malignancy which is diagnosed in more than  
42 230,000 women each year (Ferlay et al., 2015), represents a major clinical challenge. Aside from the  
43 difficulties in developing new lines of targeted treatments, late detection and lack of understanding of  
44 the molecular mechanisms that drive development of the disease remain major hurdles. Studies in  
45 BRCA1/2 germline mutation carriers undergoing prophylactic cancer risk-reducing surgery (Callahan et  
46 al., 2007; Leeper et al., 2002) identified distinct early malignant changes in the distal part of the FT,  
47 leading to wide-spread acceptance of the theory that the FT is the primary tissue of origin of HGSOC  
48 (Bowtell et al., 2015; Vaughan et al., 2011). These lesions, termed **Small Tubal Intraepithelial**  
49 **Carcinoma (STIC)**, are also routinely detected in the FT epithelium of ~50 % of patients at an advanced  
50 stage of the disease, and were shown to have the same genomic profile as the mature cancer -  
51 indicative of a clonal relationship (Kuhn et al., 2012). Nevertheless, all tumor samples genetically and  
52 transcriptionally cluster together and closely resemble tubal epithelium, irrespective of whether STICs  
53 were detected in the FT (Ducie et al., 2017). Therefore, it remains unclear how cellular transformation  
54 occurs, and most importantly, which factors are essential for the development of invasive and  
55 metastatic properties, which are necessary for the spread of malignant cells from the FT to the ovary  
56 and beyond. Of particular interest in this context is the role of mutant p53, which is almost universally  
57 detected in metastatic HGSOC cancers (Cancer Genome Atlas Research Network, 2011), but can  
58 occasionally be found in the form of p53 signatures in healthy patients with unclear clinical significance  
59 (Lee et al., 2007). Thus, it cannot be excluded that the occurrence of mutated p53 is coupled to  
60 additional, independent transformation stimuli that provide a selective advantage during the process  
61 of transformation.

62 The recently reported generation of organoid cultures from ovarian cancer (Kopper et al., 2019),  
63 confirmed that this 3D *in vitro* model recapitulates the major properties of the cancer found *in vivo*.  
64 While providing a comprehensive overview of the different histological subtypes and stages of the  
65 disease, almost all primary HGSOC samples used in this study were pre-exposed to neoadjuvant  
66 chemotherapy. Thus, it remains unclear how stem cell regulation is altered in the native HGSOC tumor  
67 tissue compared to healthy epithelium. Here we defined growth conditions needed to achieve long-  
68 term expansion of HGSOC organoids from primary tumor deposits. We show that the niche  
69 requirements for cultivation of cancer organoids differ markedly from the growth conditions for  
70 maintaining epithelial homeostasis in healthy FT organoids, which depend on active Wnt and Notch as  
71 well as inhibited BMP paracrine cascades as previously established (Kessler et al., 2015).

72 In total, we have created 15 stable organoid lines from 13 primary deposits of advanced HGSOC  
73 patients, which match the mutational and phenotypic profile of the parental tumor. Importantly,

74 long-term growth of engineered FT organoids with simultaneous depletion of p53, PTEN and RB  
75 could be sustained only in medium adapted for patient-derived HGSOC organoids. Comparative gene  
76 expression analysis of cancer organoids and p53/PTEN/RB triple knockdowns under different growth  
77 conditions revealed common key regulatory changes in markers of stemness and differentiation. This  
78 implies that signaling cues from the stem cell environment need to change early during  
79 tumorigenesis to facilitate the growth of mutated cells, and are preserved in the advanced disease  
80 setting. Thus, this study discovers important core principles in the development of HGSOC, which  
81 have important implications for understanding early carcinogenesis and disease progression.

82

### 83 **Results**

#### 84 **Establishment of HGSOC organoid culture**

85 In order to define conditions for long-term *in vitro* propagation of primary cancer organoids from solid  
86 HGSOC deposits, we utilized a combinatorial screening approach, using samples obtained during  
87 primary debulking surgery. To avoid potential contribution from healthy fallopian tube or ovarian  
88 surface epithelium, only tumor samples from peritoneum and omentum deposits were used. The  
89 tissue was not pre-exposed to pharmacological agents, as all but one HGSOC patient underwent radical  
90 surgery prior to chemotherapy, in line with local clinical guidelines. Overall, 15 organoid lines were  
91 established from 13 different patients, which were classified based on TNM and FIGO staging  
92 (Supplementary Table 1). The majority had cancer deposits >2 cm that had invaded organs outside the  
93 pelvis (T3c) and spread to retroperitoneal lymph nodes (N1), but had not metastasized to more distant  
94 sites such as the liver and spleen (M0) (Fig. 1A). In order to generate a reference data set for each  
95 organoid line, the parental tumor sample was divided into 3 parts for 1) confirmation of the diagnosis  
96 by an experienced pathologists using histological analysis of standard HGSOC biomarkers (Supp. Fig.  
97 1A), 2) isolation of DNA and RNA, and 3) isolation of cells for organoid culture (Fig. 1B).

98 By testing media containing different combinations of growth factors (Fig. 1C) we identified conditions  
99 that support outgrowth and long-term expansion (>1 year) of cancer-derived organoids. Normal FT  
100 organoid medium (FTM) is supplemented with ROCK and TGF- $\beta$  receptor inhibitors, as well as Noggin,  
101 EGF, FGF, RSPO1 and Wnt3a (Kessler et al., 2015; Kopper et al., 2019). By contrast, HGSOC organoids  
102 did not grow in this medium but required several alterations. The only paracrine growth factor that  
103 proved indispensable was EGF (E). Most notably, unlike healthy organoids from several different  
104 organs (intestinal, FT, gastric, liver etc), which require exogenous Wnt activation, not a single organoid  
105 line could be maintained in medium containing the Wnt signalling agonist Wnt3a (W) (Fig. 1C and  
106 Supplementary Table 2). Two lines did, however, expand in the presence of the Wnt agonist R-spondin  
107 1 (RSPO1, short R), suggesting that some cultures benefit from the addition of RSPO (Fig. 1C). In

108 addition, sustained inhibition of BMP signalling by Noggin (N) seems to be detrimental, as removal of  
109 inhibitor was a prerequisite for successful cultivation in 13/15 HGSOC samples, indicating  
110 fundamentally different roles of BMP and Wnt signalling in the regulation of stemness in HGSOC  
111 compared to normal tissue. In summary 11/15 cultures could be initiated and expanded in medium  
112 containing EGF, ROCK and TGF- $\beta$  inhibitor, but without Noggin – thus allowing endogenous BMP  
113 signalling. 5 of these 11 samples benefited from the addition of BMP2 for organoid formation, further  
114 amplifying BMP signalling (B). As this patient-dependent effect of BMP2 addition was always neutral  
115 or positive, BMP2 was subsequently included in the standard medium composition. Therefore, the  
116 combination of EGF and BMP2, together with the common components of the organoid cultures  
117 ROCK, TGF- $\beta$  inhibitor B27, N2 and nicotinamide was termed ovarian cancer medium (OCM).

118 Successfully established long-term HGSOC organoid cultures were passaged at a ratio of 1:2 to 1:3  
119 every 10-20 days for at least 5 months prior to cryopreservation. Six lines were kept in culture for >1  
120 year (Supplementary Table 2). Thawed cancer organoids could routinely be expanded to a multi-well  
121 screening format, and are thus suited for generating live biobanks of HGSOC organoids to explore  
122 individual therapeutic options *in vitro*.

123 Immunofluorescence labelling confirmed that the organoids exhibit all hallmarks of an HGSOC  
124 phenotype, including disorganized tissue architecture and loss of polarity (as marked by the absence  
125 of a central cavity), an epithelial secretory identity of all cells (strong EpCAM and PAX8 expression),  
126 and pleomorphic nuclei (Fig. 1D). HE staining further confirmed their morphological similarity to the  
127 matching tissue samples (Fig. 1E). Moreover, as proof-of-concept of the applicability of HGSOC  
128 organoids for translational research, we tested the *in vitro* drug response to carboplatin, the major  
129 first-line chemotherapeutic agent for HGSOC. As expected, organoids underwent cell death in a  
130 concentration-dependent manner, with prominent differences between organoids from different  
131 donors confirming individual variation in drug response among patients (Fig. 1F and Supp. Fig. 1B).

132

### 133 **HGSOC organoids match tumor tissue in mutational profile and expression of biomarkers.**

134 To test whether patient-derived organoid cultures correspond to the individual mutational profile of  
135 the parental tumor, we performed targeted sequencing for 121 candidate genes that were selected  
136 on the basis of previously published studies of ovarian cancer genomic profiles (Supplementary Table  
137 3) (Cancer Genome Atlas Research Network, 2011; Norquist et al., 2018). Mutational analysis of 10  
138 paired tumor fragments and organoids from 9 different patients revealed that despite the long-term  
139 expansion *in vitro*, they retained a high level of similarity, even including allelic frequency (Fig. 2A and  
140 Supplementary Table 4). *TP53* mutations were detected in the vast majority of samples (9/10), in  
141 agreement with the almost universal occurrence of mutated p53 in HGSOC patients (Cancer Genome

142 Atlas Research Network, 2011). All of the *TP53* mutations in the organoid cultures were homozygous  
143 (<0.9 allele frequency), yet diverse with respect to mutation type (missense, nonsense, frame-shift or  
144 splice variant mutations). In addition to somatic mutations with proven tumorigenic potential, a  
145 number of known variant alleles were identified, including *ROCK2* (c.1292C>A), *KIT* (c.1621A>C), *MLH1*  
146 (c.655A>G) and *MSH6* (c.472C>T) which could potentially influence malignant phenotype (Brahmi et  
147 al., 2015; Kalender et al., 2010; Nakamura et al., 2014). Apart from *TP53*, *MLH1* and *MSH6*, we also  
148 found point mutations in other genes with functions in DNA repair and chromosome stability, including  
149 *ATM* (c.4534G>A), *ATR* (c.1517A>G), *BRIP1* (c.254T>A) and *FANCA* (c.1238G>T). Interestingly, while no  
150 classic germline or somatic *BRCA1/2* mutations were detected apart from three polymorphisms that  
151 are weakly associated with ovarian cancer (c.4900A>G, c.3113A>G, c.2612C>T), analysis of protein  
152 lysates revealed a significant reduction compared to healthy FT organoids in 3 of 8 cases (OC4, OC2  
153 and OC3; Suppl. Fig. 2A). This strongly suggests the existence of epigenetic, or post-transcriptional  
154 mechanisms of *BRCA1* inactivation in these cases. Altogether, 7/9 patients had mutations in one or  
155 more DNA repair gene, in congruence with the fact that HGSOC is a cancer characterized by a  
156 particularly high incidence of genomic instability. Given our finding that HGSOC organoids could not  
157 be maintained in the presence of Wnt, we noted with interest that 3 missense mutations in Wnt  
158 pathway genes (*Fzd9*, *LRP5*, *TCF7L2*) were identified in 3 different patients (Fig. 2A), which could impair  
159 signal transduction and thus provide further evidence that changes in this pathway play an important  
160 role in ovarian carcinogenesis. Complementary to the sequencing data, WB and IF staining were  
161 performed to examine the mutational status and subcellular localization of p53 in the organoids  
162 (Supplementary Table 4). While the nonsense mutation in OC11 as well as the splice variant and frame-  
163 shift mutations in OC4 and OC7, respectively, result in loss of p53 (Fig. 2B and Supplementary Table 5),  
164 the missense mutations in OC9 (p.R273H), OC10 (p.R175H), OC1 (p.V25F) and OC6 (p.V173M) result in  
165 a gain-of-function and nuclear accumulation phenotype with R273H and R175H being two of the most  
166 common mutations in ovarian cancer (Zhang et al., 2016) (Fig. 2C and Suppl. Fig. 2B).

167 To more thoroughly evaluate parallels between tissue and organoid cultures, a global gene expression  
168 analysis was performed from 8 different tumor/organoid pairs as well as 3 healthy FT tissue/organoid  
169 pairs and 2 FT organoids derived from cancer patients (also classified as normal healthy tissue). The  
170 generation of a multi-dimensional-scaling plot (MDS) revealed that the distance between OC and FT  
171 organoids is smaller than between corresponding tissues, likely due to the greater complexity of tissue  
172 samples, which contain mesenchymal and endothelial components (Fig. 2D). Still, despite the tissue  
173 heterogeneity, the respective OC organoids express very similar levels of the main cancer markers, like  
174 *CDKN2A* (p16), *Muc16* and *EpCAM*, when compared to the parental sample (Fig. 2E). Moreover,  
175 correlation analysis of FT and OC organoids (Supp. Fig. 2B) shows that FT samples form a homogenous

176 cluster and show less variability in gene expression between each other than OC organoids, which  
177 instead reflect the phenotypic diversity of ovarian tumors.

178 A thorough analysis of gene expression revealed that numerous hallmark genes known to be de-  
179 regulated in HGSOC are differentially expressed between OC and normal FT samples, not only in the  
180 tissue but also in organoids (Fig. 2F). This includes significant up-regulation of the cell cycle regulators  
181 CDKN2A and Cyclin E1 (CCNE1) and the transcription factor FOXM1, as well as down-regulation of  
182 differentiation markers like PGR and OVGPI.

183 The strong up-regulation of CCNE1 was validated by western blot analysis in 5 out of 8 samples tested  
184 (Supp. Fig. 2C and D), while RB protein itself, which is phosphorylated by CCNE1 to promote G1/S  
185 progression, was not differentially expressed (data not shown). This indicates potential RB pathway  
186 disruption by increased CCNE1 levels. Amplification of CCNE1 gene is common in HGSOC (~20-30% of  
187 cases) but increased levels could also be a result of alternative signalling perturbations.

188 Together these results demonstrate that the patient-derived OC organoid lines are valid *in vitro* models  
189 of the parental HGSOC tumors, resembling not only the tissue architecture but also the mutational  
190 profile and overall gene expression.

191

## 192 **Stable triple knockdown of p53, PTEN and RB in FT organoids**

193 In the next step, we wanted to analyze at which stage of disease development the observed changes  
194 in niche factor requirements occur. This is a question of particular importance in HGSOC, where  
195 transformation appears to occur in the FT but cancers are very rarely detected at this site. To mimic  
196 the cellular events, like mutation of p53 and loss of PTEN, which characterize the early stages of  
197 malignant transformation *in vitro*, we used organoids from healthy FT donor epithelium. In contrast to  
198 previous tumorigenesis models based on the transformation of immortalized primary FT monolayers  
199 (Jazaeri et al., 2011; Nakamura et al., 2018), organoids are genetically unaltered and have preserved  
200 epithelial polarity and integrity, thus ensuring mucosal homeostasis.

201 In order to model HGSOC development, shRNAs against p53, PTEN, and RB - the major known tumour  
202 drivers of the disease - were introduced into healthy human FT epithelial cells from donor tissues  
203 obtained during surgeries for benign gynecological conditions. The shRNAs were delivered sequentially  
204 by retro- and lentiviral vectors into epithelial cells grown in 2D culture, selected by FACS (shPTEN-  
205 mCherry, shRB-GFP) and subsequently transferred to Matrigel to initiate organoid formation (Fig. 3A  
206 and Suppl. Fig. 3A). Among the double-positive mCherry/GFP population (shPTEN, shRB), p53 depleted  
207 organoids were selected with puromycin. Successful knockdown of all 3 target genes was confirmed  
208 on RNA as well as protein level (Fig. 3B). In total 7 triple knockdown (KD) cultures were successfully

209 generated from different FT donor tissue confirming robustness of the methodology (Suppl. Fig. 3D).  
210 In congruence with the downregulation of RB and PTEN protein, functional analysis of triple KD  
211 organoids revealed an increase in expression of CCNE1 (Fig. 3C) and elevated levels of activated  
212 phosphorylated Akt (pAkt), respectively (Suppl. Fig. 3B). Depletion of p53 protein was confirmed by  
213 resistance of organoids to the MDM2 inhibitor Nutlin3A, which triggers apoptosis in p53 WT cells  
214 (Suppl. Fig.3C).

215 We next compared phenotypes of KD and WT organoids by confocal microscopy. We observed loss of  
216 cell shape and misalignment of the nuclei, indicative of changes in the maintenance of apico-basal  
217 polarity – although the organization of the monolayer remained intact and the lumen was preserved  
218 with a cystic growth of the organoids. Triple KD cells also showed a stronger signal for the DNA damage  
219 marker γH2AX, indicating an increased frequency of DNA double-strand breaks and thus suggesting  
220 genomic instability (Fig. 3D). Notably, KD organoids had enlarged and polymorphic nuclei, which is one  
221 of the prominent morphological characteristics of HGSOC cells (Fig. 3D). While all these phenotypic  
222 changes suggest that the knockdown of p53, PTEN, and RB in FT organoids is pro-carcinogenic, none is  
223 sufficient as bona fide evidence of malignancy. Indeed KD cells remained competent to undergo  
224 differentiation into ciliated cells, which are thought to be the terminally differentiated cells of the FT  
225 (Fig. 3E).

226

## 227 **Rescue of KD organoid lines in ovarian cancer medium**

228 Despite an initial growth advantage until the first passage after seeding, KD organoids cannot be  
229 maintained in long-term culture and undergo growth arrest after 4-8 passages, as shown by the growth  
230 curve in comparison to WT and vector control (Fig. 4A and Suppl. Fig. 4A). While individual differences  
231 among different donor cultures were observed, the premature growth arrest of KD organoids was  
232 confirmed in 7/7 cases (Suppl. Fig. 3D). This suggests that the KD organoids may undergo similar  
233 changes in stemness regulation as those observed in the HGSOC organoids.

234 Indeed, growing the organoids in ovarian cancer medium improved organoid formation efficiency and  
235 enabled long-term growth (Fig. 4B). Importantly, long-term growth could only be rescued if OCM was  
236 added at passage 0/1, suggesting that inadequate niche conditions lead to irreversible loss of  
237 stemness. Phase contrast images (Suppl. Fig. 4B) confirm that while individual organoids grow to a  
238 similar size, organoid numbers are lower at each passage in FTM, finally resulting in premature growth  
239 arrest. Western blot analysis of γH2AX and cleaved caspase 3, as well as PARP1, indicated that the  
240 growth-suppressive effect of Wnt3a did not result from direct cytotoxicity, as DNA damage and  
241 apoptosis was not reduced when organoids were grown in OCM (Fig. 4C and Supp. Fig. 4C). Single p53  
242 or double p53/PTEN KD on the other hand did not exhibit increased γH2AX levels, irrespective of the

243 medium used, indicating that the enhanced DNA damage observed in triple KDs is the result of RB  
244 depletion.

245 In order to discover factors induced by culture in OCM that contribute to maintenance of stemness  
246 and longevity of the triple KD and HGSOC organoids, we performed global gene expression analysis. As  
247 expected, OCM medium devoid of Wnt and RSPO1 led to a reduction in the expression of Wnt target  
248 genes in both organoids (Suppl. Fig. 4D). The microarray data also reveal that despite cell growth arrest  
249 of the KD organoids in FTM, they continue to show elevated expression of classical HGSOC markers,  
250 including FOXM1, TOP2A, CDKN2A, and WT1, albeit at lower levels than when grown in OCM (Fig. 4D).  
251 This finding proves that knockdown of key tumor suppressor genes is sufficient to induce a degree of  
252 cellular transformation towards a cancer phenotype and supports the view that the FT epithelium is  
253 the tissue of origin of HGSOC.

254 However, a clear increase in the expression of genes related to stemness (CD133, MycN and SOX2) and  
255 a decrease in genes related to differentiation (PGR, OVGP1, and FOXJ1) was found in KD organoids  
256 grown in OCM vs. FTM (Fig. 4E). While PGR and ESR1 are differentiation markers connected to  
257 hormone signaling, FOXJ1 is the major transcription factor required for ciliogenesis and thus  
258 development of motile ciliated cells, presumed to be the terminally differentiated cell type in the FT  
259 mucosa. The downregulation of FOXJ1 compared to the vector control was validated by RT-PCR for  
260 organoids from 2 patients (Fig. 4F). In addition, quantification of immunolabelling against dtTubulin  
261 (Fig. 4G) in 3 independent organoid lines confirmed a lack of ciliated cells in the triple KD organoids  
262 grown in OCM, but not in FTM. Since FT mucosa renewal is driven by the differentiation of bipotent  
263 progenitors (Ghosh et al., 2017; Kessler et al., 2015), the absence of ciliated cells is suggestive of a shift  
264 towards the secretory phenotype. Notably, an outgrowth of secretory cells is thought to be a critical  
265 step in the development of HGSOC from FT epithelium. Our findings indicate that this process can be  
266 triggered *in vitro* by p53/PTEN/RB depletion, provided that canonical Wnt pathway activation is  
267 reduced.

268

### 269 **Wnt free medium supports stemness of HGSOC and KD organoids**

270 Next, we wanted to confirm independently that Wnt-free medium increases stemness of KD organoids.  
271 FACS analysis of the bona fide OC stem cell marker CD133 (Kryczek et al., 2012), which is expressed on  
272 the cell surface, revealed that the number of positive cells in triple KD organoids increased when  
273 cultured in OCM vs FTM (Fig. 5A and Supp. Fig. 5A). In vector ctrl and WT cells, by contrast, the number  
274 of CD133+ cells was lower in OCM, consistent with FTM providing more optimal conditions for the  
275 preservation of stemness in healthy epithelial cells. Loss of stemness coincides with a reduction in  
276 growth potential as quantified by a luciferase-based assay determining the number of live cells after

277 two passages of parallel cultivation in the different media (Fig. 5B). This confirms that the presence of  
278 Wnt agonists in the environment hampers the growth of p53/PTEN/RB KD organoids by repressing  
279 stemness – indicative of a substantial change in stemness regulation.

280 To substantiate these results, we analyzed the direct effect of Wnt3a/RSPO1 supplementation on  
281 patient-derived HGSOC organoid growth and CD133 expression. Differential treatment of cancer  
282 organoids over 2 passages clearly showed that addition of these Wnt agonists to OCM resulted in a  
283 highly significant ( $p < 0.0001$ ) inhibition of organoid growth, an effect confirmed for all 6 OC organoid  
284 lines tested (Fig. 5C). Interestingly, the inhibitory effect of noggin on already established cultures was  
285 mild, but significant, confirming that BMP pathway activity is beneficial for growth but not as essential  
286 as for initial organoid formation. However, addition of noggin to mature organoid lines had no effect  
287 on the number of CD133+ cells, while Wnt3a/RSPO1 reduced numbers significantly (Fig. 5D and Supp.  
288 Fig. 5B), strongly suggesting that canonical Wnt pathway activation negatively regulates stemness in  
289 HGSOC organoids via CD133 expression.

290 As Wnt3a supplementation relies on the addition of conditioned medium from a Wnt-producing cell  
291 line, we next wanted to confirm that its effect was specific to the presence of Wnt. Indeed, Wnt-  
292 conditioned medium strongly upregulated the established Wnt target gene AXIN2 (Suppl. Fig. 5C). In  
293 addition, medium conditioned by the parental cell line without the Wnt-producing vector (CM) did not  
294 negatively affect organoid growth (Fig. 5E).

295 Overall, it can be concluded that the presence of Wnt ligands, which induce a signature of canonical  
296 Wnt target gene expression in KD and HGSOC organoids, results in a striking decrease of stemness and  
297 growth capacity in these cultures.

298

### 299 **MYCN and Wnt inhibitors are upregulated in HGSOC and KD FT organoids**

300 The data from HGSOC organoids provide strong evidence that the mechanisms by which growth of  
301 cancer organoid stem cells is maintained are altered from those in the healthy epithelium and our  
302 experiments with KD organoids further show that depletion of only three tumor-driver genes can  
303 recapitulate this effect. To get a better insight into putative candidate genes that could contribute to  
304 the maintenance of stemness in cancer organoids, we compared microarray data of healthy FT  
305 epithelium and HGSOC tissue as well as patient-derived cancer and KD organoids grown in OC vs FT  
306 medium (Fig. 6A). The proto-oncogene MYCN was uniformly upregulated in cancer tissue, as well as  
307 triple KD organoids cultured in OCM, suggesting that it may play a role in driving stemness and cancer  
308 growth in HGSOC. qPCR confirmed MYCN expression to be significantly higher in cancer organoids  
309 compared to FT organoids (Fig. 6B, left panel). In addition, expression levels of MYCN relative to GAPDH

310 were validated by qPCR in 3 independent biological replicates of triple KD organoids cultured in OCM  
311 vs. FTM (Fig. 6B, right panel).

312 In line with our finding that suppression of canonical Wnt signaling supports the growth of cancer  
313 organoids, the gene expression data revealed enhanced expression of the Wnt inhibitors KREMEN2  
314 and DKK3 in both triple KD and OC organoids (Fig. 6A). While KREMEN2 regulation appears to be driven  
315 by changes in the genetic background, DKK3 expression seems to be induced by Wnt-free medium.  
316 Therefore, it appears that the altered paracrine signaling environment further promotes inhibition of  
317 canonical Wnt signaling. Interestingly, downregulation of p53/PTEN/RB in FT organoids caused a  
318 decrease in Wnt target gene expression even in the presence of Wnt3a and RSPO1 (Fig.6C), while  
319 culture in Wnt-free medium leads to a further strong reduction of LEF1 and TCF transcripts down to  
320 the detection limit of the microarray (see Supplementary Table 6). The expression of Wnt inhibitors  
321 and the reduced Wnt signaling induced by tumor suppressor KD are in agreement with our hypothesis  
322 that Wnt pathway suppression is required for HGSOC growth. Interestingly, HGSOC organoids  
323 expressed increased levels of differentiation markers when exposed to Wnt3a/RSPO1. In line with the  
324 microarray results and data from the triple KD organoids, RT-PCR confirmed increased expression of  
325 the ciliogenesis factor FOXJ1 in cancer organoids cultured in the presence of Wnt3a/RSPO1 (Fig. 6D).  
326 Based on this, we postulate a two-step process of HGSOC development in which changes in the niche  
327 environment are a necessary step that drives dedifferentiation and maintains stemness in cells bearing  
328 tumorigenic mutations.

329

330

331 **Discussion**

332 Our understanding of the cellular mechanisms that underlie the development of HGSOC in the FT and  
333 its spread to the ovaries and beyond remains rudimentary and represents a major obstacle to advances  
334 in diagnosis and therapy. Although some properties of cancer stem cells in HGSOC have been described  
335 (Choi et al., 2015; Lupia and Cavallaro, 2017; McLean et al., 2011), there is no knowledge about the  
336 intrinsic mechanisms that drive tumor growth and mediate recurrent disease. As patients frequently  
337 receive neoadjuvant chemotherapy prior to debulking surgery, such tumor samples are likely to  
338 already show secondary biological alterations. This study thus provides systematic insight into the  
339 biology of HGSOC organoids derived directly from debulking surgery samples, which reflect the biology  
340 of the initial cancer tissue.

341 In contrast to the healthy FT epithelium (Kessler et al., 2015), we find that HGSOC cancer organoids  
342 require a low Wnt signaling environment but an active BMP signaling axis. Wnt independence was  
343 previously observed in other cancers such as pancreas and colon (Fujii et al., 2016; Seino et al., 2018)  
344 and positively correlates with the stage of metastatic disease. However, in contrast to organoids from  
345 other cancers, e.g. metastatic pancreatic cancer, which do not require Wnt but do grow in  
346 Wnt/Noggin/Rspo medium, exogenous supplementation of Wnt3a actually prevented formation and  
347 growth of all HGSOC cancer organoids. Recently, Kopper et al (2019) also reported the use of Wnt-free  
348 medium for the generation of HGSOC organoids but attributed negative effect of Wnt to the potential  
349 contaminating presence of serum without testing the hypothesis. Here we clearly show that lack of  
350 exogenous Wnt signaling is in fact a requirement for maintaining stemness and preventing  
351 differentiation in HGSOC and that pro-cancerous mutations by themselves are therefore likely not  
352 sufficient to drive transformation of healthy epithelium. Thus, it is tempting to speculate that the  
353 overall environment in the FT epithelium (with presumably high Wnt signaling) represses cancer  
354 outgrowth and promotes escape of (pre)-malignant cells to more distant sites, like the surface of the  
355 ovaries and peritoneum. Interestingly, even formation of the two organoid cultures that benefited  
356 from the presence of RSPO1 (Figure 1) could be efficiently prevented by addition of Wnt3a and noggin,  
357 suggesting high sensitivity of the HGSOC organoids to elevated Wnt signaling. Nevertheless, these  
358 cases show that the heterogeneity of this disease warrants routine testing of two different media  
359 during establishment of fresh cultures: OCM and OCM + RSPO1 and FGF.

360 Our analysis of HGSOC and KD organoids clearly demonstrates that a high Wnt environment leads to  
361 the downregulation of stemness genes and the upregulation of differentiation genes. Mouse lineage  
362 tracing data previously showed that active Wnt signaling is required both for renewal of Pax8 secretory  
363 cells and their differentiation to ciliated cells (Ghosh et al., 2017). Our data strongly suggest that the  
364 regulation of these processes becomes separated during carcinogenesis. While Wnt stimulation still

365 induces differentiation and ciliogenesis in cancer organoids, it inhibits stemness and expansion  
366 capacity. The same effect is observed in triple KD organoids, indicating that depletion of key tumor  
367 driver proteins is sufficient to induce these alterations in stem cell regulation. Yet, despite the change  
368 in growth requirements, the prominent occurrence of nuclear atypia, increase of DNA damage and  
369 changes in epithelial organization, triple KD organoids maintained key elements of epithelial polarity.  
370 Therefore, it appears they have not completed the process of transformation and that additional  
371 changes are needed for malignancy to develop. This is also in line with the observation that growth  
372 rescue in OCM medium was incomplete. Unlike the stable long-term expansion of HGSOC organoids,  
373 which were routinely cultured for over 1 year without changes in growth dynamics, the lifespan of KD  
374 organoids in OCM was limited to 7-8 months.

375 Our data illustrate the critical importance of the model system when studying processes of cell  
376 transformation *in vitro*. Several previous studies on the putative role of the FT as the tissue of origin of  
377 HGSOC showed the transformation potential of human FT epithelial cells in 2D cell culture by  
378 overexpression of different oncogenes (h-RAS, c- MYC) followed by xenograft transplantation (Jazaeri  
379 et al., 2011; Karst et al., 2011). We show that robust regulatory mechanisms in the intact epithelium  
380 prevent the breakdown of the epithelial organization despite functional inactivation of the key HGSOC  
381 drivers p53, PTEN, and RB. Breakdown of apicobasal polarity is an important step in the emergence of  
382 many cancers, as it precedes EMT and thus facilitates cancer progression (Huber et al., 2005; Ozdamar  
383 et al., 2005). While our microarray data revealed important similarities in gene expression profile  
384 between KD FT organoids and mature cancer organoids, further studies are needed to elucidate the  
385 exact mechanism of cancer stem cell maintenance in HGSOC. MYCN, which in the absence of Wnt was  
386 ubiquitously upregulated in all OC and KD FT organoids in our study, was previously implicated as a  
387 driver of stemness in aggressive glioblastoma (Yang et al., 2017). The high degree of consistency in  
388 MYCN regulation in KD FT and HGSOC organoids from independent donor samples warrants further  
389 studies to investigate its potential role as a stemness marker in HGSOC.

390 Despite immense efforts to establish new *in vitro* models of HGSOC (Hill et al., 2018), a successful  
391 model for long-term expansion of solid tumor deposits has been missing until now. This is likely due to  
392 the altered stem cell niche requirements we describe here. Our preliminary tests with carboplatin  
393 showed individual differences in drug response of organoids from different patients, suggesting that  
394 the model is suitable for personalized therapeutic strategies. However, to define to which extent  
395 organoids are predictive of *in vivo* patient responses, more comprehensive studies in correlation with  
396 long-term clinical outcome are needed. It is possible that including other cell types in the organoid  
397 model, such as stromal and immune cells, could further advance its capacity to generate data which  
398 are predictive of clinical responses in patients (Neal et al., 2018).

399 Overall this study provides important insight into fundamental biological processes of HGSOC  
400 development. We show that functional inactivation of key tumor drivers fails to induce a direct growth  
401 advantage of the altered cells in the absence of appropriate changes in the stem cell niche  
402 environment. The existence of such a two-component mechanism opens up important new questions  
403 for understanding the etiology of HGSOC – in particular which cellular and physiological mechanisms  
404 in the tissue surrounding the FT epithelium are responsible for the critical changes in paracrine  
405 signaling that favour the outgrowth of mutated cells. In this context, the regulatory role of the  
406 neighboring ovary could further be of pivotal relevance, particularly in light of epidemiological data  
407 showing a strong correlation between inflammatory processes associated with ovulation and the risk  
408 for HGSOC development.

409

410 **Acknowledgements**

411 We would like to thank Susan Jackisch, Ina Wagner, Jörg Angermann and Oliver Thieck for technical  
412 support, Dr Gabriela Vallejo Flores, Toralf Kaiser and Jenny Kirsch for technical help with FACS  
413 experiments, Diane Schad for expert help with generating graphics and Dr. Rike Zietlow for editing the  
414 manuscript.

415

416 **Author contributions**

417 M.K. and T.F.M. conceived the project; M.K. and K.H. designed experiments, which were conducted  
418 by, K.H., M.K and S.T.; H.K. designed and planned targeted sequencing, performed by T.Z. H.B. and T.Z.  
419 analyzed the targeted sequencing data. H.B. and H.-J.M. analyzed microarray data. S.D.E and E.T  
420 performed pathology analysis of the tissue samples. M.M., selected patients and provided human FT  
421 samples J.S. and E.B. selected the patients, provided material, and clinical data of primary HGSOC  
422 patients. T.F.M. supported the project financially; K.H, M.K. and T.F.M. wrote the manuscript, M.K. and  
423 T.F.M. supervised the project.

424

425 **Declaration of Interests**

426 The authors declare no competing interests.

427

428

429 **Figure Legends**

430 **Figure 1. Establishment of patient-derived organoids from solid HGSOC deposits.**

431 A) Summary of cancer patient data with TNM and FIGO classifications showing advanced stage of  
432 disease at the time of surgery.

433 B) Graphic representation of the standard experimental procedure for tumor patient material.  
434 Samples were obtained at the time of primary debulking surgery from the high purity tumor  
435 deposits in peritoneum/omentum.

436

437 C) *In vitro* niche dependency of HGSOC tumor cells. Phase contrast pictures illustrate that isolated  
438 ovarian cancer cells rely on EGF supplementation for growth, while they do not grow at all in  
439 Wnt3a supplemented medium. Also, inhibition of BMP signalling through Noggin has strong  
440 negative effect on the initial growth. E – EGF, F – FGF10, N –Noggin, R – R-spondin1, B – Basic  
441 medium, P - Passage

442 D) Cancer organoids express HGSOC markers Pax8 and EpCAM and have lost the cystic phenotype  
443 suggesting complete breakdown of epithelial polarity as seen on confocal images from two  
444 representative organoid lines.

445 E) H&E staining of organoids and respective tissue confirm high similarity in cellular structure and  
446 tissue organization.

447 F) HGSOC organoids show differential response to Carboplatin treatment, confirming patient-  
448 specific sensitivity of the cultures. Cell viability assay was performed after 5 days of treatment  
449 with different concentrations of Carboplatin on mature organoids from three different donors.  
450 Data represent mean  $\pm$ SD of technical triplicates.

451

452 **Figure 2. HGSOC organoids match tumor tissue in mutational profile and gene expression  
453 biomarkers.**

454 A) Overview of mutations found in organoid cultures and matching tumor tissue obtained by  
455 targeted sequencing of >200 HGSOC related genes confirms almost identical profile between  
456 parental tissue and *in vitro* long-term organoid culture. Color code indicates type of mutations  
457 which were detected.

458 B) Representative western blot showing loss or overexpression of p53 in individual organoid lines

459 C) Strong nuclear p53 signal in IF stainings of HGSOC organoids is indicative of a gain-of-function  
460 *TP53* mutation. Scale bars: 100  $\mu$ m (Tissue) and 50  $\mu$ m (Organoid).

461 D) Multi-Dimensional-Scaling (MDS) plot based on the gene expression profiles (microarrays) of  
462 3 healthy FT and 8 tumor tissue samples and their respective organoid cultures shows 4  
463 clusters: Normal FT tissue, normal FT organoids, cancer organoids and cancer tissue.

464 E) Box plots depicting overall constant level in normalized expression of major HGSOC marker  
465 genes between organoids and parental tissue. Data represent the median, quartiles,  
466 maximum, and minimum of the normalized expression from 8 different donors.

467 F) Heat map of differentially expressed genes between cancer and healthy tissue/organoids  
468 reveals upregulation of several HGSOC biomarkers and reduction of FT differentiation markers  
469 in the cancer samples. Differential expression determined by single-color microarray for 8  
470 different patient samples was significant for all genes with  $p < 0.05$  except for OVGP1 and  
471 TOP2A in organoids.

472

473 **Figure 3. Stable triple knockdowns of tumor suppressors p53, PTEN and RB in healthy FT organoids.**

474 A) Experimental approach for genetic manipulation of FT epithelial cells (FTECs). FTECs were  
475 sequentially transduced in 2D culture with replication-deficient viruses containing specific  
476 shRNAs and different selection markers. After sorting cells were seeded in Matrigel for  
477 organoid formation.

478 B) Confirmation of robust knockdowns of p53, PTEN and RB in FT organoids on RNA and protein  
479 level. Relative mRNA levels were normalized to the WT mRNA level and are given as the mean  
480  $\pm$ SEM from 3 different donors. A representative western blot from one donor is depicted. RNA  
481 as well as protein samples were taken at passage 1 or 2 of each organoid line. KD – Knockdown,  
482 Vec Ctrl – Vector Control, WT- Wild type

483 C) Cyclin E1 (CCNE1) overexpression as a downstream effect of RB knockdown was confirmed by  
484 western blot analysis.

485 D) Confocal images of triple KD organoids reveal increased DNA damage ( $\gamma$ H2AX, marked by  
486 asterisks), atypic nuclei (Draq5) and loss of apicobasal polarity. Scale bar: 20 $\mu$ m.

487 E) Presence of ciliated cells (arrowheads), as revealed by IF staining against detyrosinated (dtyr)  
488 Tubulin in triple KD organoids, proves capacity for terminal differentiation. Scale bar: 50 $\mu$ m.

489

490 **Figure 4. Triple KD organoids show improved growth in ovarian cancer medium**

491 A) In long-term 3D culture triple KD organoids show loss of growth capacity and premature  
492 growth arrest compared to the controls as indicated by the representative growth curves of  
493 FT234.

494 B) Growth curves and phase-contrast images of triple KD organoids grown in OCM compared to  
495 FTM reveal successful rescue of long-term growth capacity.

496 C) Levels of DNA damage (γH2AX) and apoptosis (cleaved caspase-3, PARP1) do not differ among  
497 the different media as shown by representative western blots comparing triple KD organoids  
498 and their controls.

499 D) Triple KD (p53/PTEN/RB) organoids are characterized by a HGSOC gene expression signature  
500 as revealed by microarray analysis comparing WT and KD organoids grown in either OCM or  
501 FTM. Differential expression determined by dual-color microarray for 2 biological replicates  
502 was significant for all genes with  $p < 0.00005$ .

503 E) Differential expression of stemness- and differentiation-related genes of triple KD organoids  
504 grown in OCM vs. FTM. Fold-changes were derived from microarray data and indicate an  
505 increase in stemness (CD133, SOX2, MYCN) and a drop in differentiation under OCM conditions  
506 (OVGP1, PGR, FOXJ1). Differential expression determined by dual-color microarray for 2  
507 biological replicates was significant for all genes with  $p < 0.05$ .

508 F) FOXJ1 expression determined by qRT-PCR was significantly diminished in triple KD organoids  
509 grown in OCM compared to FTM, suggesting a decrease in differentiation capacity. Data  
510 represent the mean  $\pm$ SEM from technical triplicates for two independent knockdown cultures.

511 G) Proportion of ciliated cells is significantly reduced in KD organoids under OCM growth  
512 conditions, confirming inhibition of differentiation as illustrated by confocal images. The  
513 quantification plot depicts the mean  $\pm$ SEM from 3 independent biological replicates, based on  
514 quantification of the average number of ciliated cells per counted nuclei. 1000 cells were  
515 counted per individual experiment. \* $p < 0.05$ , two-sided Student's t-test.

516

517 **Figure 5. Wnt depletion supports preservation of stemness in HGSOC organoids**

518 A) The proportion of CD133+ cells was determined by FACS analysis after growing triple KD and  
519 control cells in FTM vs. OCM for two passages. The graph is representative of two biological  
520 replicates.

521 B) Growth capacity as well as expression of stemness markers increase when KD organoids are  
522 grown in OCM medium as shown by difference in total viable cell number (representative

523 graph of 3 independent experiments). The luminescent cell viability assay was performed in  
524 triplicate and the bar plot depicts the mean  $\pm$ SEM. \* p < 0.05, two-sided Student's t-test; KD –  
525 Knockdown, Vec Ctrl – Vector Control, WT – Wild type

526 C) Phase contrast images of cancer organoids which entered growth arrest upon treatment with  
527 Wnt agonists over 2 passages (Scale bar: 500 $\mu$ m). Differences in cell number were confirmed  
528 by the respective cell viability assays (performed in technical triplicates). Data represent the  
529 mean  $\pm$ SEM for 5 different OC organoid lines (n=5). \*\*\*\* p < 0.0001, two-sided Student's t-  
530 test.

531 D) The number of CD133+ cells determined by FACS for OC7 and OC4 organoids grown in different  
532 media with or without Wnt3A/Rspo1 and with or without Noggin over 2 passages, confirms a  
533 sharp drop in stemness in the presence of Wnt agonists.

534 E) Addition of conditioned medium collected from the parental Wnt3a cell line did not suppress  
535 growth of cancer organoids, proving that the growth inhibitory effect is due to the presence  
536 of Wnt agonists. The bar plot represents the mean  $\pm$ SEM of technical triplicates performed  
537 with a luminescent cell viability assay. \* p < 0.05, \*\*\*\* p < 0.0001, two-sided Student's t-test.

538

539 **Figure 6. Unifying induction of MYCN and Wnt inhibitors in HGSOC and KD samples.**

540 A) Comparative analysis of microarray data revealed consistent up-regulation of MYCN, the  
541 canonical Wnt inhibitors KREMEN2 and DKK3 as well as differentiation marker FOXJ1, AR and  
542 PGR in HGSOC cancer organoids as well as triple KD FT organoids. Differential expression was  
543 determined either by single-color microarray for the cancer samples (8 replicates) or dual-  
544 color microarray for the knockdowns (2 replicates) and is significant for all genes with p < 0.05.

545 B) Transcriptional induction of MYCN is confirmed by qRT-PCR for three patients between cancer  
546 organoids and normal FT organoids as well as triple KD organoids grown in OCM vs. FTM  
547 conditions. Depicted is the mean  $\pm$ SEM of the normalized MYCN mRNA expression level of  
548 three biological replicates (n=3). \*\* p < 0.01, \*\*\* p < 0.001, two-sided Student's t-test.

549 C) Microarray data revealed that expression levels of Wnt target genes are downregulated in  
550 triple KD compared to WT control organoids. Differential expression determined by dual-color  
551 microarray for 2 biological replicates was significant for all genes with p  $\leq$  0.005.

552 D) FOXJ1 expression was upregulated in ovarian cancer organoids in FTM compared to OCM as  
553 shown by qRT-PCR analysis of 3 different patient samples. Data represent the mean  $\pm$ SEM of  
554 technical triplicates.

555

556 **Materials and Methods**

557 **Fallopian tube and ovarian cancer primary patient material**

558 Approval for the preparation and experimental usage of the primary material was given by the Ethics  
559 Commission of the Charité, Berlin (EA1/002/07) and informed consent was obtained from every  
560 patient.

561 Human fallopian tube samples were provided by the Auguste-Viktoria Klinikum Berlin, Department of  
562 Gynecology and Obstetrics after standard surgical procedures for benign gynecological disease. Only  
563 anatomically normal fallopian tubes were used. The tubes were transported and dissected within 2 to  
564 3 h of removal. Of each FT sample one piece was saved for RNA/DNA preparation. After washing with  
565 DPBS, FT tissue was incubated in collagenase I (Sigma) for 45-60min at 37°C for enzymatic detachment  
566 of epithelial progenitors. Subsequently, the mucosal cells were scraped off the muscularis with a  
567 scalpel and pelleted by centrifugation (7min, 300xg). Cells were seeded in 2D culture (in ADF+++ with  
568 Pen/Strep, hEGF and ROCK inhibitor) before transfer into Matrigel™ for organoid formation.

569

570 Ovarian cancer tissue was received from the Department of Gynecology, Charité University Hospital,  
571 Campus Virchow Clinic. Cancer samples, surgically removed from patients with a preliminary diagnosis  
572 of HGSOC were retrieved from tumors of specified sites within the abdominal cavity. The tumor  
573 material was transported and processed within few hours after surgery and each sample was divided  
574 into 3 pieces for cell preparation, tissue fixation and RNA/DNA isolation. For isolation of HGSOC  
575 progenitors, the tissue pieces were washed with DPBS, minced with a scalpel into very small pieces  
576 and incubated in a 1:1 mixture of collagenase I and II (Sigma) for around 60 min at 37°C on a shaker.  
577 Afterwards, the enzyme-tissue mixture was vortexed to further separate the cells. Next, the cell  
578 suspension was centrifuged (5 min, 300 x g, 4°C), resuspended in ADF+++ supplemented with  
579 Pen/Strep, hEGF and ROCK inhibitor and seeded in a cell culture vessel or directly in Matrigel™.

580

581 **Organoid culture of FT epithelial cells (FTECs)**

582 The organoids were cultured as described in Kessler et al (2015). In brief, to initiate organoid growth  
583 approximately 30,000 cells obtained from 2D culture, were seeded in 50 µL Matrigel™ and overlaid  
584 with a growth factor cocktail stimulating different paracrine pathways including EGF and Wnt  
585 signalling. The composition for normal FT epithelial cell medium (FTM) was as follows: ADF, 25%  
586 conditioned Wnt3A-medium and 25 % conditioned RSPO1 medium, supplemented with 12 mM HEPES,  
587 1% GlutaMAX™, 2% B27, 1% N2, human EGF, human noggin, human FGF-10, 1 mM nicotinamide, 9  
588 µM ROCK inhibitor (Y-27632) and 0.5 µM TGF-β RI Kinase Inhibitor IV (SB431542).

589 Medium was changed every 3-4 days and organoids were expanded every 2-3 weeks at a rate of 1:2  
590 to 1:3. To do so, organoids were released from Matrigel<sup>TM</sup>, washed with ADF++, taken up in pre-  
591 warmed TrypLE<sup>TM</sup> and incubated for 7-10 min at 37 °C for enzymatic digestion. Subsequently, organoids  
592 were vortexed, washed with ADF++ and pelleted. Finally, the shredded organoids were resuspended  
593 in fresh Matrigel<sup>TM</sup> and seeded into pre-warmed cell culture plates before FTM was added to the  
594 organoids.

595

596 **Organoid culture of ovarian cancer cells**

597 After initial isolation from the tumor tissue, ovarian cancer cells were seeded in Matrigel<sup>TM</sup> at a  
598 concentration of approx. 30,000 cells/50 µl. Because cancer cells did not form organoids or were  
599 difficult to expand in FTM, different media compositions were tested to support *in vitro* growth. The  
600 basic medium for the ovarian cancer organoids always contained the following supplements and  
601 growth factors: ADF supplemented with 12 mM HEPES, 1% GlutaMAX<sup>TM</sup>, 2% B27, 1% N2, human EGF,  
602 1 mM nicotinamide, 9 µM ROCK inhibitor (Y-27632) and 0.5 µM TGF-β RI Kinase Inhibitor IV  
603 (SB431542). Upon proper organoid maturation and growth under specified conditions they were split  
604 at a ratio of 1:3 every 1-2 weeks. To expand the OC organoids they were released from Matrigel<sup>TM</sup>  
605 using ice-cold ADF++, centrifuged and resuspended in pre-warmed TrypLE<sup>TM</sup>. Enzymatic digestion was  
606 carried out for 7 min at 37 °C. Afterwards, the organoid suspension was vortexed, mixed with cold  
607 ADF++ and centrifuged (300xg, 5 min). Next, the supernatant was removed, the cell pellet resuspended  
608 in Matrigel<sup>TM</sup> and seeded into pre-warmed cell culture plates. After ~20 min the Matrigel<sup>TM</sup> was  
609 overlaid with the respective medium. The medium was changed twice per week and the organoids  
610 kept in a humidified incubator at 37 °C and 5% CO<sub>2</sub>.

Medium/Supplement	Provider (Cat. no.)	Final conc.
<b>Advanced DMEM/F12 (ADF)</b>	Gibco (12634)	
<b>B27 supplement</b>	Gibco (17504044)	1x
<b>BMP2, human</b>	Gibco (PHC7146)	10 ng/ml
<b>EGF, human</b>	Gibco (PHG0311)	10 ng/ml
<b>Fetal calf serum (FCS)</b>	Biochrom (S0115)	5 or 10%
<b>FGF-10, human</b>	Peprotech (100-26-B)	100 ng/ml
<b>GlutaMax</b>	Gibco (35050-038)	1x
<b>HEPES</b>	Gibco (15630-056)	12 mM
<b>N2 supplement</b>	Gibco (17502048)	1x
<b>Nicotinamide</b>	Sigma-Aldrich (N0636)	10 mM
<b>Noggin, human</b>	Peprotech (120-10C)	100 ng/ml
<b>Nutlin3a</b>	Sigma (N6287)	5-10 $\mu$ M
<b>Penicillin/Streptomycin</b>	Gibco (15140-122)	100 U/ml 10 mg/ml
<b>Puromycin</b>	Gibco (A11138-03)	0.5 $\mu$ g/ml
<b>Y-27632 dihydrochloride monohydrate (ROCK inhibitor)</b>	Chemdea (CD0141)	9 $\mu$ M
<b>Rspo-1</b>	In-house production Cell line: 293T HA Rspo1-Fc	10-25% (v/v)
<b>SB431542 (TGF-<math>\beta</math> inhibitor)</b>	Calbiochem (616454)	0.5 $\mu$ M
<b>Wnt3a</b>	In-house production (Willert et al. 2003) Cell line: L Wnt-3a (ATCC® CRL-2647™)	10-25% (v/v)

611

612 **Organoid stocks**

613 Organoid stocks were prepared by releasing organoids from ~1 week-old confluent cultures in cold  
614 ADF++, pelleting by centrifugation and resuspension in the freezing medium CryoSFM. After transfer

615 of the organoid suspension into cryotubes and a freezing container, stocks were kept at least 24 h at -  
616 80 °C before transfer into liquid nitrogen for long-term storage.

617

618 **Cloning of shRNAs and virus production**

619 To obtain stable knockdowns of PTEN and RB (in-house-designed) shRNA sequences targeting specific  
620 regions within the respective mRNA were cloned into the lentiviral vector pLVTHM (Addgene#12247)  
621 carrying mCherry or GFP as mammalian selection marker. Cloning included the following steps: 1.  
622 *Clal/Mlul* (NEB) restriction of pLVTHM-GFP or -mCherry vector, 2. Annealing of sense and antisense  
623 oligos (target sequence with specific overhangs), 3. Ligation of the linearized vector and annealed  
624 oligos (Quick ligation kit, NEB) and 4. Transformation into *E.coli*. The retroviral vector with the shRNA  
625 against p53 was provided by Alexander Loewer.

626

627 **Replication-deficient retro- and lentiviral particles were produced** by transient transfection of 293T  
628 cells using FuGENE® 6 reagent (Promega). In brief, specific amounts of viral target and packaging  
629 plasmids were mixed with Opti-MEM™ (Thermo Scientific). Next, a mixture of Opti-MEM™ and  
630 FuGENE® 6 was added to the plasmids and incubated for 20-30 min at RT. The formed liposomes were  
631 added dropwise to 293T cells (~75% confluence) in 1xDMEM (supplemented with 2 mM L-glutamine,  
632 1mM Na-pyruvate and 10% FCS). The next day (~12 h), the transfection medium was aspirated and  
633 fresh medium added. Around 36-48h post-transfection the viral supernatant was collected, filtered  
634 (0.45 µm) and concentrated with Lenti-X™ concentrator (Clontech). The viral pellet was resuspended  
635 in ADF medium to achieve 10x concentrated virus. Aliquots were stored at -80°C.

636 **Lentiviral vectors:** psPAX2 (packaging plasmid; Addgene#12260), pMD2.G (VSV-G envelope plasmid;  
637 Addgene#12259), pLVTHM-GFP (Addgene#12247), pLVTHM-GFP/mCherry-Luci (shRNA against  
638 luciferase as control vector; target sequence (5'-3'): *AACTTACGCTGAGTACTTCGA*), pLVTHM-mCherry-  
639 PTEN (pLVTHM-mCherry with shRNA against PTEN; target sequence (5'-3'): *AGGCGCTATGTGTATTATTAT*), pLVTHM-GFP-Rb (pLVTHM-GFP with shRNA against Rb; target sequence  
640 (5'-3'): *GGTTGTAATGGCCACATATAG*)

642 Retroviral vectors were a gift by Alexander Loewer and plasmids are described in Brummelkamp et al.  
643 (2002) (retroviral packaging plasmid, retroviral envelope plasmid, pSUPER.retro (Addgene#3926),  
644 pSUPER.retro.p53 (pSUPER.retro with shRNA against p53; target sequence (5'-3'): *GACTCCAGTGGTAATCTAC*)

646 **Genetic manipulation of primary cells**

647 To genetically modify primary FT epithelial cells, they were treated with retro-and lentiviruses in 2D  
648 culture. Freshly isolated FECs of an early passage (p0/p1) were transduced when reaching around 50-  
649 70% confluence with 1x concentrated virus diluted in ADF+++ and supplemented with hEGF and 5 µg/µl  
650 polybrene (Sigma). The cells were incubated for 12-18 h with the viral suspension. The next day, the  
651 supernatant was removed and fresh 2D medium added to the cells. When the cultures reached 80-  
652 90% confluence they were split with TrypLE™ and seeded back into 2D at a ratio of 1:2 to 1:3. In the  
653 next passage the second virus was added in the same manner. Cells were sequentially transduced and  
654 expanded until they reached max. passage 3.

655 To retrieve successfully transduced cells carrying a fluorescent selection marker, FACS was performed.  
656 For this purpose, the primary cells were detached using TrypLE™ (~10 min), pelleted by centrifugation  
657 (5min, 300xg), resuspended in FACS buffer (1xDPBS with 1% FCS, 1% HEPES and 3% ROCK inhibitor)  
658 and passed through a 35 µm cell strainer into polystyrene tubes.

659 Propidium iodide (Sigma) was added shortly before FACS to exclude the dead cells. Sorting was  
660 performed by the Flow cytometry core facility (DRFZ, Charitéplatz 1, 10117 Berlin) using the FACSAria  
661 II (BD). The GFP and mCherry single or double-positive cells were collected in polystyrene tubes  
662 supplied with 2D medium. Collected cells were centrifuged directly after FACS and seeded in 3D culture  
663 with around  $1.5 \times 10^5$  cells/ 50 µl Matrigel™. Cells transduced with the retroviral vector were selected  
664 by adding 0.5 µg/ml puromycin (Gibco) for 10 days to the respective cell culture.

665

### 666 **Single cell preparation and flow cytometry**

667 To prepare single cells, organoids were released from Matrigel™ using cold PBS, pelleted by  
668 centrifugation (5 min, 300xg), resuspended in TrypLE and incubated for 15-20 min at 37 °C. After  
669 enzymatic treatment and vortexing, the organoid fragments were further mechanically disrupted by  
670 passing 3-4x through a needle (26G). Next, the cells were taken up in ADF and passed through a 40 µm  
671 filter. The single-cell suspension was pelleted and washed by addition of 1% BSA in PBS. The cells were  
672 stained in 1xPBS with 1-2% BSA. Staining was performed for 10-30 min at 4 °C in the dark. Finally, the  
673 cells were washed and resuspended in 1xPBS. Flow cytometric analysis was performed using a  
674 FACSCanto™ II (BD) or LSRFortessa™ (BD) flow cytometer and the FlowJo vX.0.6 software.

675

### 676 **Cell viability assay**

677 To quantify the number of viable cells within one organoid well, we applied the CellTiter-Glo® 3D Cell  
678 Viability Assay (Promega # G9681). The assay was carried out according to the manufacturers' protocol

679 and the luminescence was measured within 30 min after the start of the reaction using black 96-well  
680 plates (Costar®, Corning) and a standard plate reader.

681

## 682 **Immunohistochemistry of HGSC tissue**

683 Paraffin-embedded tumor samples in 5 µm sections was stained with the mouse monoclonal  
684 antibodies EpCam (clone VU-1D9, Thermoscientific, Thermo Fischer Scientific, Waltham,  
685 Massachusetts, USA) at 1:100, for p16 (clone 16P04, NeoMarkers, Fremont, California, USA) at 1:600,  
686 for p53 (clone DO-7, Dako, Carpinteria, California, USA) at 1:50 dilution and for Pax8 (clone MRQ-50,  
687 Cell Marque by Sigma-Aldrich, Rocklin, California, USA) at suppliers instructions on the Ventana  
688 Benchmark XT Autostainer instrument (Ventana Medical Systems, Inc., Tucson, AZ, USA). 3, 3'-  
689 diaminobenzidine peroxide substrate (DAB<sup>+</sup>) of the “ultraView Universal DAB detection kit” (Ventana)  
690 was used as a chromogen. Signals were strong and clearly discernable and furthermore well-  
691 established in our diagnostic routine laboratory.

692

## 693 **Immunofluorescence staining**

694 For fixation organoids were released from Matrigel and incubated in 3.7% PFA for ~1 h at RT, while  
695 tissue pieces were incubated in PFA for ~24 h at RT. Organoids and tissues were then dehydrated and  
696 paraffinized. For dehydration organoids were passed manually through an alcohol dilution series: 60%  
697 EtOH (20 min, RT), 75% EtOH (20 min, RT), 90% EtOH (20 min, RT), abs. EtOH (20 min, RT), 100%  
698 isopropanol (20 min, RT) and 2x 100% acetone (20 min, RT). Tissue pieces were transferred to the  
699 Shandon Citadell 1000 rondell for automatic dehydration. After dehydration, organoids and tissue  
700 pieces were embedded in paraffin, sectioned at 5 µm and collected onto microscope slides.

701 Prior to staining, the formaldehyde-fixed paraffin-embedded (FFPE) organoids and tissues were  
702 deparaffinized by applying a series of decreasing alcohol concentrations: xylene (2x 10 min), 100%  
703 ethanol (2x 2 min), 90% ethanol (1x 2 min), 70% ethanol (1x 2 min), 50% ethanol (1x 2 min) and H<sub>2</sub>O  
704 (2x 2 min). For antigen retrieval the slides were incubated for 30 min at 98 °C in 1x Target retrieval  
705 solution (Dako). Sections were stained by adding primary antibodies diluted in immunofluorescence  
706 buffer (IFB: 1% BSA, 2% FCS and 0.1% Tween-20 in 1xPBS) and depending on the antibody incubated  
707 for 90 min at RT or overnight at 4°C in a humidified chamber. After washing 5x 5 min with 1x PBS  
708 supplemented with 0.05% Tween-20, the respective secondary antibodies diluted in IFB together with  
709 the nucleic acid dye DRAQ5 or Hoechst were added to each section and incubated for 60 min at RT.  
710 Subsequently, the slides were washed and sections mounted on coverslip using Mowiol.

Primary Antibody	Provider (Cat. no.)	Application (dilution)
<b>BRCA1</b>	Santa Cruz (sc-642)	WB (1:200)
<b>Cyclin E1 (CCNE1)</b>	Cell Signaling (4219)	WB (1:1000)
<b>Cleaved Caspase-3 (Asp175)</b>	Cell Signaling (9661)	WB (1:1000)
<b>detyrosinated Tubulin</b>	Abcam (ab48389)	IF (1:100)
<b>E-cadherin</b>	BD Biosciences (610181)	IF (1:100)
<b>EpCAM (VU1D9)</b>	Cell Signaling (2929)	IF (1:100)
<b>P53 (1C12)</b>	Cell Signaling (2524)	IF (1:2000)
<b>P53 (DO-1)</b>	Santa Cruz (sc-126)	WB (1:500)
<b>PARP</b>	Cell Signaling (9542)	WB (1:2000)
<b>PAX8</b>	Proteintech (10336-1-AP)	IF (1:50)
<b>phospho γH2AX (Ser139)</b>	Cell Signaling (9718)	IF (1:480); WB (1:1000)
<b>PTEN</b>	Cell Signaling (9552)	WB (1:1000)
<b>Rb (4H1)</b>	Cell Signaling (9309)	WB (1:2000)
<b>CD133/1 (AC133)- APC</b>	Miltenyi Biotec (130-090-826)	FC (1:100)
<b>IgG1-APC (isotype)</b>	Miltenyi Biotec (130-098-846)	FC (1:100)

711

## 712 **H&E-Staining**

713 Before staining with haematoxylin and eosin (H&E), organoid slices were deparaffinized as described  
714 above. After deparaffinization, the sections were covered completely with Mayer's haematoxylin  
715 solution (Roth) and incubated for 15 min at RT. The slides were rinsed with ddH<sub>2</sub>O and tap water.  
716 Subsequently, the sections were covered with Eosin Y solution (1% aqueous, Roth) and incubated for  
717 10 min at RT. Finally, slides were rinsed for 1 min with ddH<sub>2</sub>O and embedded using Roti®-Histokitt.

718

## 719 **Quantitative Reverse-Transcription PCR (qRT-PCR)**

720 The AB Power SYBR® Green RNA-to-CT™ 1-Step Kit (Thermo Fisher) was applied to perform reverse  
721 transcription and quantitative PCR in one step. RNA was added in a volume of 10 µl at a concentration  
722 between 2-10 ng/µl. qRT-PCR was performed using the StepOnePlus™ Real-Time PCR System (Applied  
723 Biosystems) with the following program: 1. 30 min, 48 °C; 2. 10 min, 95 °C; 3. 15 sec, 95 °C and 4. 1

724 min, 60 °C. Steps 3 and 4 were repeated 40 times. For each primer pair and RNA-sample the reaction  
725 was done in triplicate. The amplification plots obtained from the qRT-PCR were analyzed with the  
726 StepOne™ Software (version 2.3; Thermo Fisher). The expression levels were relatively quantified by  
727 calculating  $\Delta\Delta C_t$ . The expression levels of the target genes were always normalized to the expression  
728 of the housekeeping gene glyceraldehyde-3-phosphate dehydrogenase (GAPDH).

729 Primer sequences (5'-3'): GAPDH\_for – GGTATCGTGGAAAGGACTCATGAC; GAPDH\_rev –  
730 ATGCCAGTGAGCTTCCGTTCAAG; Ki67\_for – AAGCCCTCCAGCTCCTAGTC; Ki67\_rev –  
731 TCCGAAGCACCACTTCTTCT; FOXJ1\_for – GGAGGGGACGTAAATCCCTA; FOXJ1\_rev –  
732 GGTCCCAGTAGTTCCAGCAA; TP53\_for – CCTCCTCAGCATCTTATCCGA; TP53\_rev –  
733 TGGTACAGTCAGAGCCAACCTC; PTEN\_for – CGACGGGAAGACAAGTTCAT; PTEN\_rev –  
734 AGGTTCCCTGGTCCTGGT; RB\_for – GGAAGCAACCCTCCTAAACC; RB\_rev – TTTCTGCTTTGCATTCTG;  
735 AXIN2\_for – AGATCCAGTCGGTGATGGAG; AXIN2\_rev – CTTCATTCAAGGTGGGGAGA; MYCN\_for –  
736 CTTCGGTCCAGCTTCTCAC, MYCN\_rev - GTCCGAGCGTGTCAATTTT

737

### 738 **Western blotting**

739 For the purpose of sample collection organoids were washed with DPBS, pelleted and lysed by addition  
740 of 1x Laemmli buffer and heating for 10 min at 95 °C. After the proteins were separated according to  
741 their molecular weight by performing SDS-PAGE, they were transferred from the gel to a PVDF  
742 membrane using a Mini Trans-Blot® Electrophoretic Transfer Cell (Bio-Rad) and applying 250 mA, 400  
743 V and 4 °C under constant stirring for 2.5 h. After blocking in a mixture of 5% milk and BSA the  
744 membrane was incubated at 4 °C overnight with the primary antibody. The next day the membrane  
745 was washed 3x 10 min in TBST. Subsequently, the membrane was incubated for 1 h at RT with the  
746 respective conjugated secondary antibody. After washing, the membrane was covered with  
747 chemiluminescence reagents. Using Hyperfilm (Amersham Biosciences) and a developer machine, the  
748 proteins were visualized. The housekeeping gene  $\beta$ -actin was used as the internal control for  
749 normalization of protein loading.

750

### 751 **DNA/RNA isolation**

752 DNA was isolated using either the AllPrep DNA/RNA Mini Kit (QIAGEN) for tissue and organoids. DNA  
753 purifications were quantified by measuring optical density at 260 nm wavelengths.

754 RNA from cells of 3D cultures was isolated using the RNeasy Mini Kit (QIAGEN) or the AllPrep DNA/RNA  
755 Mini Kit (QIAGEN). RNA from tissue samples was isolated using the AllPrep DNA/RNA Mini Kit  
756 (QIAGEN). After pelleting the organoids, they were lysed in the respective sample buffer and RNA

757 purification was performed according to the manufacturer's protocols. RNA concentration and purity  
758 were measured with a NanoDrop® ND-1000 Spectrophotometer.

759 For microarray analysis total RNA was isolated with TRIzol (Life Technologies) according the supplier's  
760 protocol using glycogen as carrier. Quality control and quantification of total RNA was carried out using  
761 the NanoDrop 1000 UV-Vis spectrophotometer (Kisker) as well as the Agilent 2100 Bioanalyzer with a  
762 RNA Nano 6000 microfluidics kit (Agilent Technologies).

763

764 **Drug testing**

765 To test the response of patient-derived HGSOC organoids to the chemotherapeutic drug carboplatin  
766 (Merck), organoids were dissociated into single cells by using enzymatic (TrypLE, 15 min, 37 °C) and  
767 mechanical (vortex and passing through 26G needle) disruption. Subsequently, cells were counted and  
768 seeded at 15,000 cells/ 25µl Matrigel™ into a 48-well plate. After maturation of organoids (~7-10 days  
769 in culture) treatment with carboplatin with a concentration range between 0-100 µg/ml was started.  
770 At one week post-treatment, cell viability was determined as described above.

771

772 **Microarrays (Dua-color and Single-color)**

773 Microarray experiments were performed as dual-color or single-color hybridizations on either Agilent  
774 Whole Human Genome 4x44K microarrays (Design ID 014850) or 8x60K human custom (Agilent-  
775 048908) microarrays comprising identical features for coding genes. Color-swap dye-reversal  
776 hybridizations were performed in order to compensate for dye specific effects and to ensure  
777 statistically relevant data when using small sample sizes. RNA labeling was done either with a two-  
778 color Quick Amp Labeling Kit (4x44K arrays) or with a one-color Low Input Quick Amp Kit (8x60K arrays)  
779 according the supplier's recommendations (Agilent Technologies).

780 In brief, mRNA was reverse transcribed and amplified using an oligo-dT-T7 promoter primer and the  
781 T7 RNA polymerase. The resulting cRNA was labeled with only Cyanine 3-CTP (single-color) or with  
782 Cyanine 3-CTP and Cyanine 5-CTP (dual-color). After precipitation, purification, and quantification, 1  
783 µg (4x44K arrays) or 300 ng (8x60K arrays) of each labeled cRNA was fragmented and hybridized to  
784 whole-genome multipack microarrays according to the manufacturer's protocol (Agilent  
785 Technologies). Scanning of microarrays was performed with 5 µm resolution and XDR extended range  
786 (4x44K arrays) or 3 µm resolution (8x60K arrays) using a G2565CA high-resolution laser microarray  
787 scanner (Agilent Technologies). Microarray image data were analyzed and extracted with the Image  
788 Analysis/Feature Extraction software G2567AA v. A.11.5.1.1 (Agilent Technologies) using default

789 settings and either the GE2\_1100\_Jul11 (dual-color) or the GE1\_1105\_Oct12 (single-color) extraction  
790 protocol.

791 For analysis of dual-color microarrays the extracted MAGE-ML files were processed with the Rosetta  
792 Resolver, Build 7.2.2 SP1.31 (Rosetta Biosoftware). Ratio profiles comprising single hybridizations were  
793 combined in an error-weighted fashion to create ratio experiments. A 1.5-fold change expression cut-  
794 off for ratio experiments was applied together with anti-correlation of ratio profiles, rendering a highly  
795 significant, robust and reproducible microarray analysis (p-value < 0.01). Additionally, raw data txt files  
796 were analyzed with R packages from the Bioconductor repository.

797 The extracted single-color raw data files were background corrected, quantile normalized and further  
798 analyzed for differential gene expression using R 3.4 (Ritchie et al., 2015) (Supplementary Information  
799 Table 2 and 3). Microarray gene expression comparisons between groups and the associated  
800 BioConductor package LIMMA were performed using unpaired tests for all human comparisons (R Core  
801 Team, 2013).

802

803 **Capture of the targeted disease-related genome and Next-Generation Sequencing.** A SureSelectXT  
804 Automation Custom Capture Library (Agilent) target enrichment panel was designed. The enrichment  
805 panel comprised all coding exons of 121 genes associated with ovarian cancer (Supplementary Table  
806 3). Capture was performed according to the manufacturer's instructions using an NGS Workstation  
807 Option B (Agilent) for automated library preparation starting with 3 µg DNA per sample. Sequencing  
808 was performed on an Illumina HiSeq 2500 system generating 2x100bp paired end reads with a target  
809 coverage of >200-fold per sample. Sequence reads were mapped to the haploid human reference  
810 genome (hg19) using BWA. Single nucleotide variants (SNVs) and short insertions and deletions (indels)  
811 were called using FreeBayes v1.1. (Garrison and Marth, 2012).

812 Variants called by FreeBayes were filtered for quality (QUAL > 10, coverage > 50) and annotated by  
813 SnpEff v4.3k (Cingolani et al., 2012) and Annovar (Wang et al., 2010). For each variant the effect with  
814 the highest impact as defined by SnpEff was selected. Variants were flagged as rare if they showed less  
815 than 1% population frequency in the 1000 genome (Auton et al., 2015) and ESP6500 [Exome Variant  
816 Server, NHLBI GO Exome Sequencing Project (ESP), Seattle, URL: <http://evs.gs.washington.edu/EVS/>;  
817 accessed 2014-12] data sets. Predictions of amino acid exchange effects on protein function from  
818 MetaSVM, MetaLR and M-CAP as provided by Annovar were used to assess loss of function.

819

820 **Code Availability**

821 All code used for generating analyses used in this publication is available from  
822 [https://github.com/MPIIB-Department-TFMeyer/Hoffmann\\_et\\_al\\_Ovarian\\_Cancer\\_Organoids](https://github.com/MPIIB-Department-TFMeyer/Hoffmann_et_al_Ovarian_Cancer_Organoids).  
823

824 **References**

825 Auton, A., Brooks, L.D., Durbin, R.M., Garrison, E.P., Kang, H.M., Korbel, J.O., Marchini, J.L., McCarthy, S., McVean, G.A., and Abecasis, G.R. (2015). A global reference for human genetic variation. *Nature* 526, 68-74.

826

827

828 Bowtell, D.D., Bohm, S., Ahmed, A.A., Aspuria, P.J., Bast, R.C., Jr., Beral, V., Berek, J.S., Birrer, M.J., Blagden, S., Bookman, M.A., *et al.* (2015). Rethinking ovarian cancer II: reducing mortality from high-grade serous ovarian cancer. *Nat Rev Cancer* 15, 668-679.

829

830

831 Brahmi, M., Alberti, L., Dufresne, A., Ray-Coquard, I., Cassier, P., Meeus, P., Decouvelaere, A.V., Ranchere-Vince, D., and Blay, J.Y. (2015). KIT exon 10 variant (c.1621 A > C) single nucleotide polymorphism as predictor of GIST patient outcome. *BMC Cancer* 15, 780.

832

833

834 Brummelkamp, T.R., Bernards, R., and Agami, R. (2002). A system for stable expression of short interfering RNAs in mammalian cells. *Science* 296, 550-553.

835

836 Callahan, M.J., Crum, C.P., Medeiros, F., Kindelberger, D.W., Elvin, J.A., Garber, J.E., Feltmate, C.M., Berkowitz, R.S., and Muto, M.G. (2007). Primary fallopian tube malignancies in BRCA-positive women undergoing surgery for ovarian cancer risk reduction. *J Clin Oncol* 25, 3985-3990.

837

838

839 Cancer Genome Atlas Research Network (2011). Integrated genomic analyses of ovarian carcinoma. *Nature* 474, 609-615.

840

841 Choi, Y.J., Ingram, P.N., Yang, K., Coffman, L., Iyengar, M., Bai, S., Thomas, D.G., Yoon, E., and Buckanovich, R.J. (2015). Identifying an ovarian cancer cell hierarchy regulated by bone morphogenetic protein 2. *Proc Natl Acad Sci U S A* 112, E6882-6888.

842

843

844 Cingolani, P., Platts, A., Wang le, L., Coon, M., Nguyen, T., Wang, L., Land, S.J., Lu, X., and Ruden, D.M. (2012). A program for annotating and predicting the effects of single nucleotide polymorphisms, SnpEff: SNPs in the genome of *Drosophila melanogaster* strain w1118; iso-2; iso-3. *Fly (Austin)* 6, 80-92.

845

846

847

848 DUCIE, J., DAO, F., CONSIDINE, M., OLVERA, N., SHAW, P.A., KURMAN, R.J., SHIH, I.M., SOSLOW, R.A., COPE, L., and LEVINE, D.A. (2017). Molecular analysis of high-grade serous ovarian carcinoma with and without associated serous tubal intra-epithelial carcinoma. *Nat Commun* 8, 990.

849

850

851 Ferlay, J., Soerjomataram, I., Dikshit, R., Eser, S., Mathers, C., Rebelo, M., Parkin, D.M., Forman, D., and Bray, F. (2015). Cancer incidence and mortality worldwide: sources, methods and major patterns in GLOBOCAN 2012. *Int J Cancer* 136, E359-386.

852

853

854 Fujii, M., Shimokawa, M., Date, S., Takano, A., Matano, M., Nanki, K., Ohta, Y., Toshimitsu, K., Nakazato, Y., Kawasaki, K., *et al.* (2016). A Colorectal Tumor Organoid Library Demonstrates Progressive Loss of Niche Factor Requirements during Tumorigenesis. *Cell Stem Cell* 18, 827-838.

855

856

857 Garrison, E., and Marth, G. (2012). Haplotype-based variant detection from short-read sequencing. *arXiv:12073907 [q-bioGN]*.

858

859 Ghosh, A., Syed, S.M., and Tanwar, P.S. (2017). In vivo genetic cell lineage tracing reveals that oviductal secretory cells self-renew and give rise to ciliated cells. *Development* 144, 3031-3041.

860

861 Hill, S.J., Decker, B., Roberts, E.A., Horowitz, N.S., Muto, M.G., Worley, M.J., Jr., Feltmate, C.M., Nucci, M.R., Swisher, E.M., Nguyen, H., *et al.* (2018). Prediction of DNA Repair Inhibitor Response in Short-Term Patient-Derived Ovarian Cancer Organoids. *Cancer Discov* 8, 1404-1421.

862

863

864 Huber, M.A., Kraut, N., and Beug, H. (2005). Molecular requirements for epithelial-mesenchymal transition during tumor progression. *Curr Opin Cell Biol* 17, 548-558.

865

866 Jazaeri, A.A., Bryant, J.L., Park, H., Li, H., Dahiya, N., Stoler, M.H., Ferriss, J.S., and Dutta, A. (2011). Molecular requirements for transformation of fallopian tube epithelial cells into serous carcinoma. *Neoplasia* 13, 899-911.

867

868

869 Kalender, M.E., Demiryurek, S., Oztuzcu, S., Kizilyer, A., Demiryurek, A.T., Sevinc, A., Dikilitas, M., Yildiz, R., and Camci, C. (2010). Association between the Thr431Asn polymorphism of the ROCK2 gene and risk of developing metastases of breast cancer. *Oncol Res* 18, 583-591.

870

871

872 Karst, A.M., Levanon, K., and Drapkin, R. (2011). Modeling high-grade serous ovarian carcinogenesis from the fallopian tube. *Proc Natl Acad Sci U S A* 108, 7547-7552.

873

874 Kessler, M., Hoffmann, K., Brinkmann, V., Thieck, O., Jackisch, S., Toelle, B., Berger, H., Mollenkopf,  
875 H.J., Mangler, M., Sehouli, J., *et al.* (2015). The Notch and Wnt pathways regulate stemness and  
876 differentiation in human fallopian tube organoids. *Nat Commun* 6, 8989.

877 Kopper, O., de Witte, C.J., Lohmussaar, K., Valle-Inclan, J.E., Hami, N., Kester, L., Balgobind, A.V.,  
878 Korving, J., Proost, N., Begthel, H., *et al.* (2019). An organoid platform for ovarian cancer captures intra-  
879 and interpatient heterogeneity. *Nat Med* 25, 838-849.

880 Kryczek, I., Liu, S., Roh, M., Vatan, L., Szeliga, W., Wei, S., Banerjee, M., Mao, Y., Kotarski, J., Wicha,  
881 M.S., *et al.* (2012). Expression of aldehyde dehydrogenase and CD133 defines ovarian cancer stem  
882 cells. *Int J Cancer* 130, 29-39.

883 Kuhn, E., Kurman, R.J., Vang, R., Sehdev, A.S., Han, G., Soslow, R., Wang, T.L., and Shih Ie, M. (2012).  
884 TP53 mutations in serous tubal intraepithelial carcinoma and concurrent pelvic high-grade serous  
885 carcinoma--evidence supporting the clonal relationship of the two lesions. *J Pathol* 226, 421-426.

886 Lee, Y., Miron, A., Drapkin, R., Nucci, M.R., Medeiros, F., Saleemuddin, A., Garber, J., Birch, C., Mou, H.,  
887 Gordon, R.W., *et al.* (2007). A candidate precursor to serous carcinoma that originates in the distal  
888 fallopian tube. *J Pathol* 211, 26-35.

889 Leeper, K., Garcia, R., Swisher, E., Goff, B., Greer, B., and Paley, P. (2002). Pathologic findings in  
890 prophylactic oophorectomy specimens in high-risk women. *Gynecol Oncol* 87, 52-56.

891 Lupia, M., and Cavallaro, U. (2017). Ovarian cancer stem cells: still an elusive entity? *Mol Cancer* 16,  
892 64.

893 McLean, K., Gong, Y., Choi, Y., Deng, N., Yang, K., Bai, S., Cabrera, L., Keller, E., McCauley, L., Cho, K.R.,  
894 *et al.* (2011). Human ovarian carcinoma-associated mesenchymal stem cells regulate cancer stem cells  
895 and tumorigenesis via altered BMP production. *J Clin Invest* 121, 3206-3219.

896 Nakamura, K., Banno, K., Yanokura, M., Iida, M., Adachi, M., Masuda, K., Ueki, A., Kobayashi, Y.,  
897 Nomura, H., Hirasawa, A., *et al.* (2014). Features of ovarian cancer in Lynch syndrome (Review). *Mol  
898 Clin Oncol* 2, 909-916.

899 Nakamura, K., Nakayama, K., Ishikawa, N., Ishikawa, M., Sultana, R., Kiyono, T., and Kyo, S. (2018).  
900 Reconstitution of high-grade serous ovarian carcinoma from primary fallopian tube secretory epithelial  
901 cells. *Oncotarget* 9, 12609-12619.

902 Neal, J.T., Li, X., Zhu, J., Giangarra, V., Grzeskowiak, C.L., Ju, J., Liu, I.H., Chiou, S.H., Salahudeen, A.A.,  
903 Smith, A.R., *et al.* (2018). Organoid Modeling of the Tumor Immune Microenvironment. *Cell* 175, 1972-  
904 1988.e1916.

905 Norquist, B.M., Brady, M.F., Harrell, M.I., Walsh, T., Lee, M.K., Gulsuner, S., Bernards, S.S., Casadei, S.,  
906 Burger, R.A., Tewari, K.S., *et al.* (2018). Mutations in Homologous Recombination Genes and Outcomes  
907 in Ovarian Carcinoma Patients in GOG 218: An NRG Oncology/Gynecologic Oncology Group Study. *Clin  
908 Cancer Res* 24, 777-783.

909 Ozdamar, B., Bose, R., Barrios-Rodiles, M., Wang, H.R., Zhang, Y., and Wrana, J.L. (2005). Regulation of  
910 the polarity protein Par6 by TGFbeta receptors controls epithelial cell plasticity. *Science* 307, 1603-  
911 1609.

912 R Core Team (2013). R: A language and environment for statistical computing. R Foundation for  
913 Statistical Computing, Vienna, Austria URL <https://wwwR-projectorg/>.

914 Ritchie, M.E., Phipson, B., Wu, D., Hu, Y., Law, C.W., Shi, W., and Smyth, G.K. (2015). limma powers  
915 differential expression analyses for RNA-sequencing and microarray studies. *Nucleic Acids Res* 43, e47.

916 Seino, T., Kawasaki, S., Shimokawa, M., Tamagawa, H., Toshimitsu, K., Fujii, M., Ohta, Y., Matano, M.,  
917 Nanki, K., Kawasaki, K., *et al.* (2018). Human Pancreatic Tumor Organoids Reveal Loss of Stem Cell  
918 Niche Factor Dependence during Disease Progression. *Cell Stem Cell* 22, 454-467.e456.

919 Vaughan, S., Coward, J.I., Bast, R.C., Jr., Berchuck, A., Berek, J.S., Brenton, J.D., Coukos, G., Crum, C.C.,  
920 Drapkin, R., Etemadmoghadam, D., *et al.* (2011). Rethinking ovarian cancer: recommendations for  
921 improving outcomes. *Nat Rev Cancer* 11, 719-725.

922 Wang, K., Li, M., and Hakonarson, H. (2010). ANNOVAR: functional annotation of genetic variants from  
923 high-throughput sequencing data. *Nucleic Acids Res* 38, e164.

924 Yang, X.H., Tang, F., Shin, J., and Cunningham, J.M. (2017). A c-Myc-regulated stem cell-like signature  
925 in high-risk neuroblastoma: a systematic discovery (Target neuroblastoma ESC-like signature). *Sci Rep*  
926 7, 41.  
927 Zhang, Y., Cao, L., Nguyen, D., and Lu, H. (2016). TP53 mutations in epithelial ovarian cancer. *Transl*  
928 *Cancer Res* 5, 650-663.

929

# Figure 1. Establishment of patient derived organoids from solid HGSOC deposits

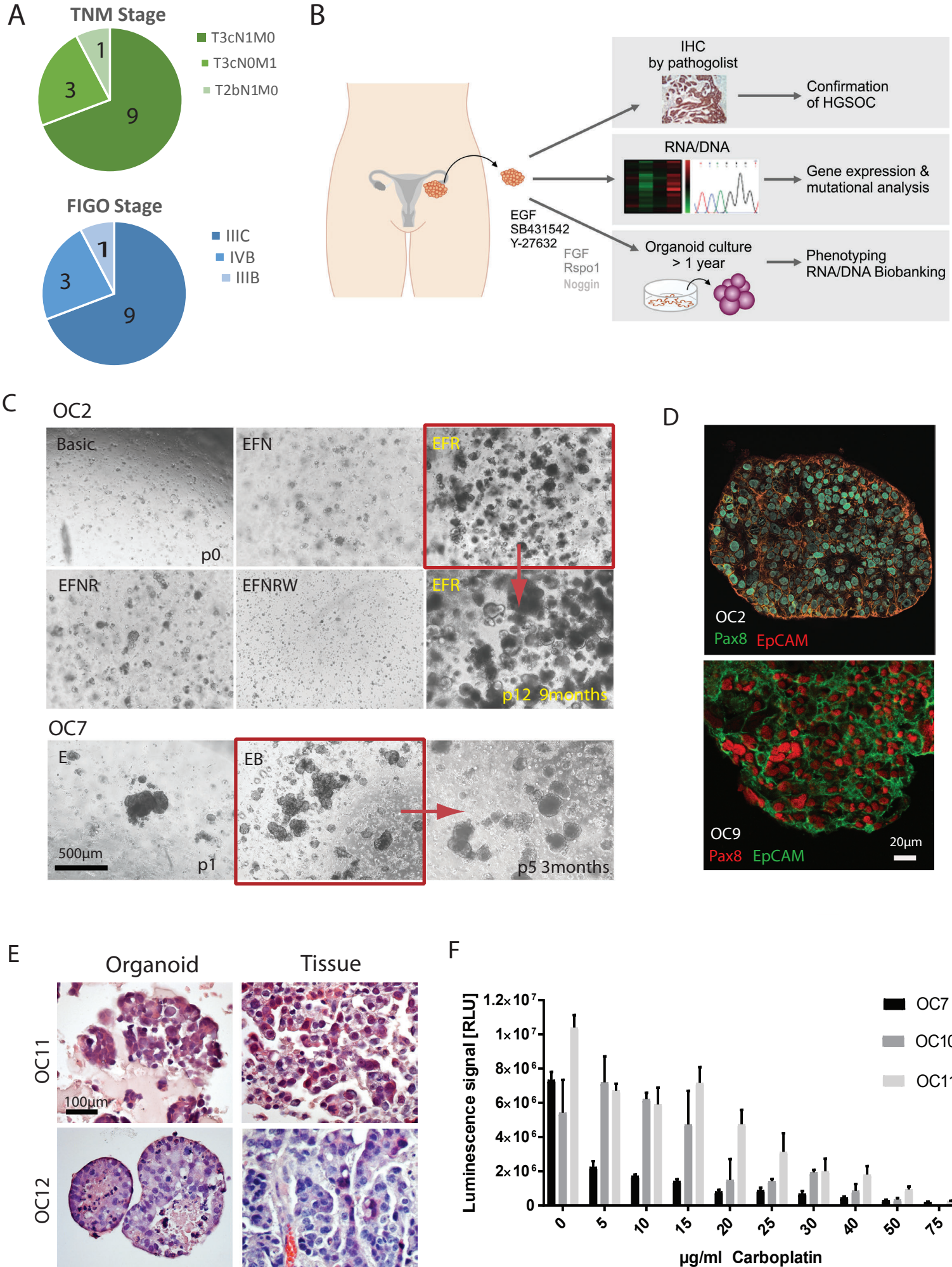
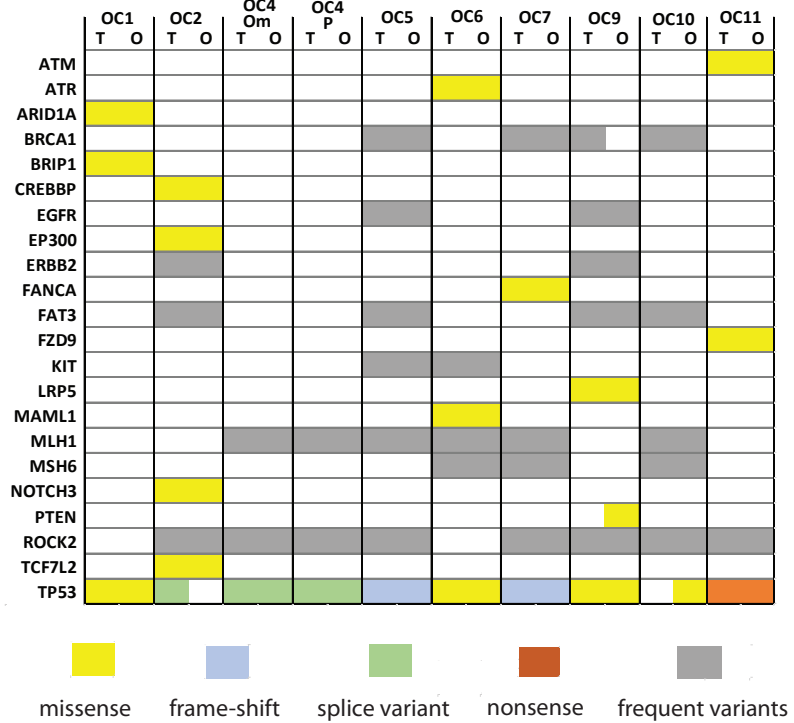
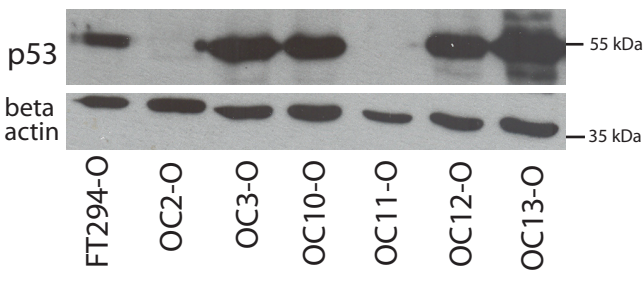


**Figure 2. HGSOC organoids match tumor tissue gene mutation profiles and gene expression markers.**

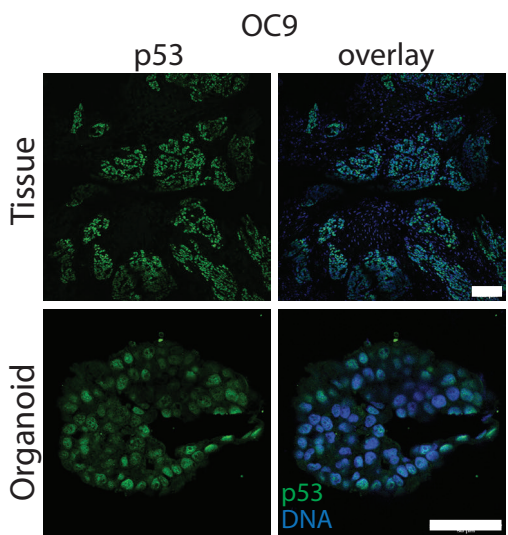
**A**



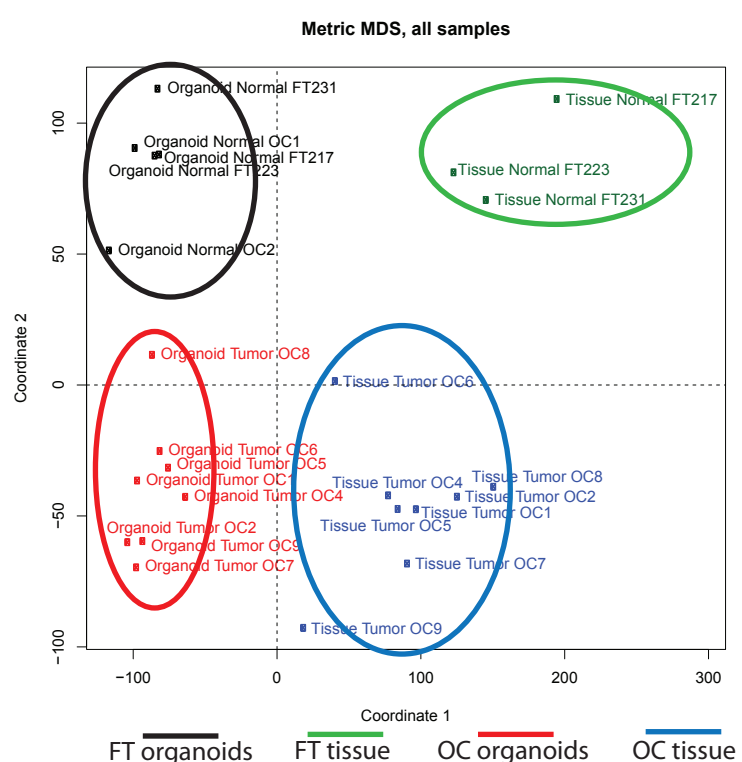
**B**



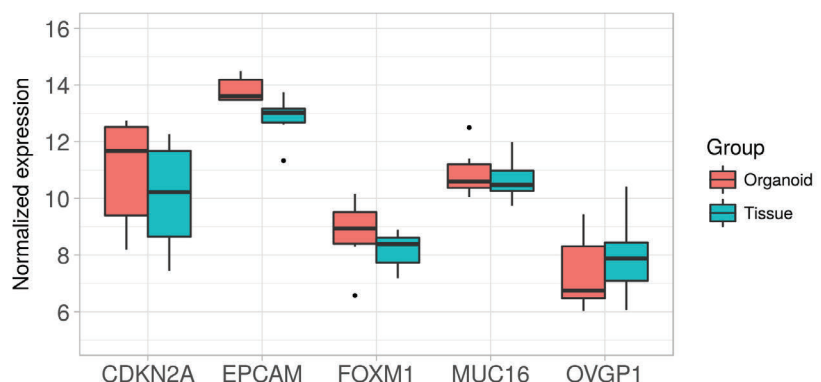
**C**



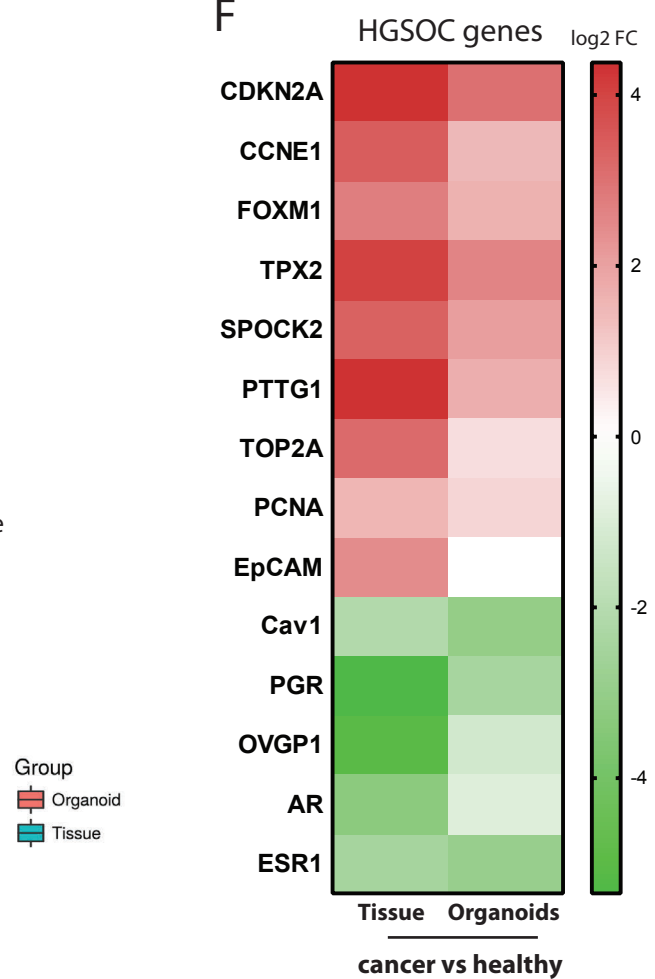
**D**



**E**

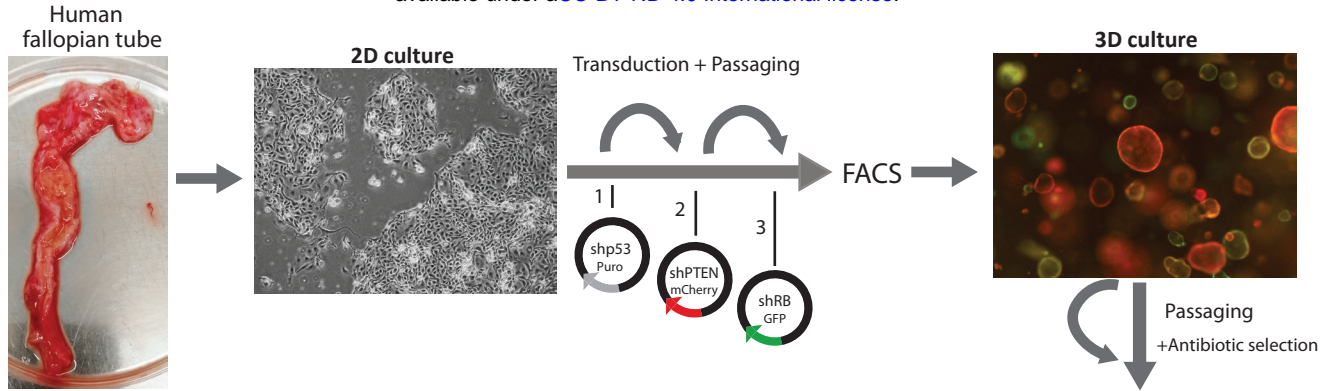


**F**

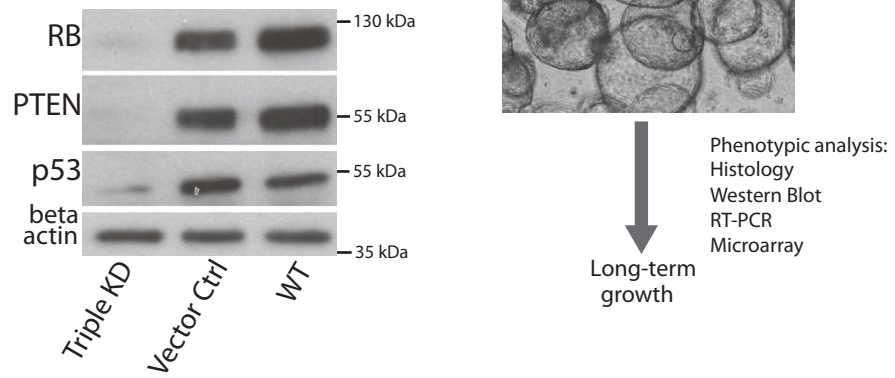
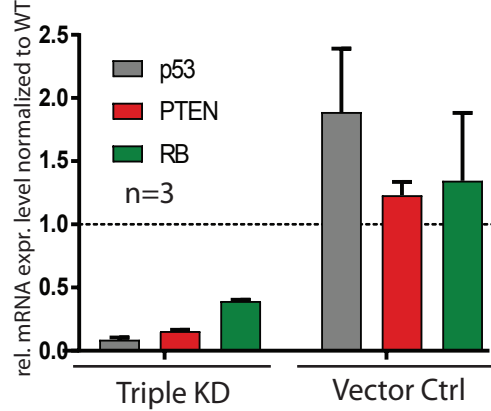


**cancer vs healthy**

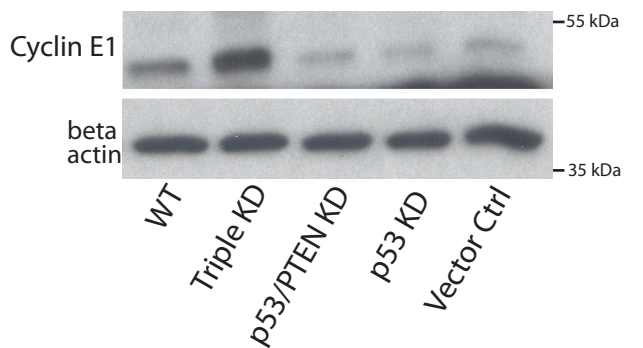
A



B



C



D

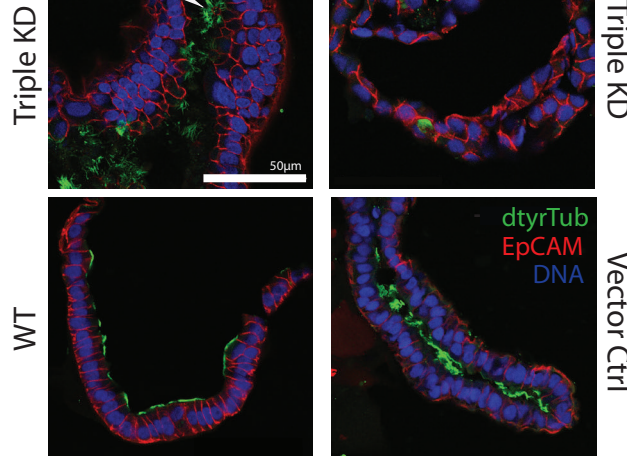
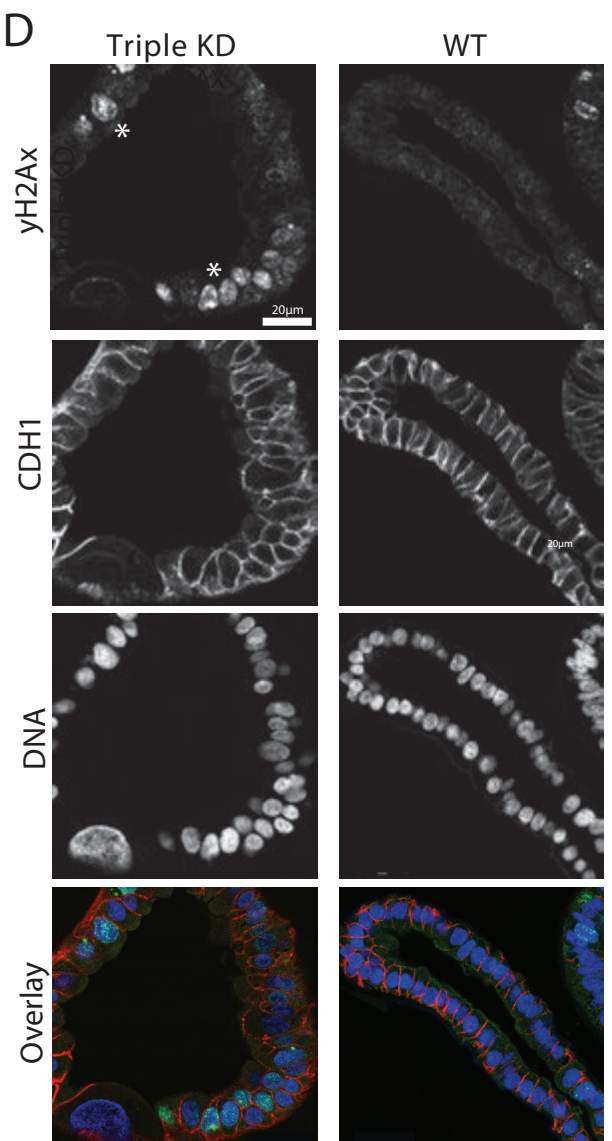


## Figure 4. Rescue of knockdown ovarian lines in ovarian cancer medium

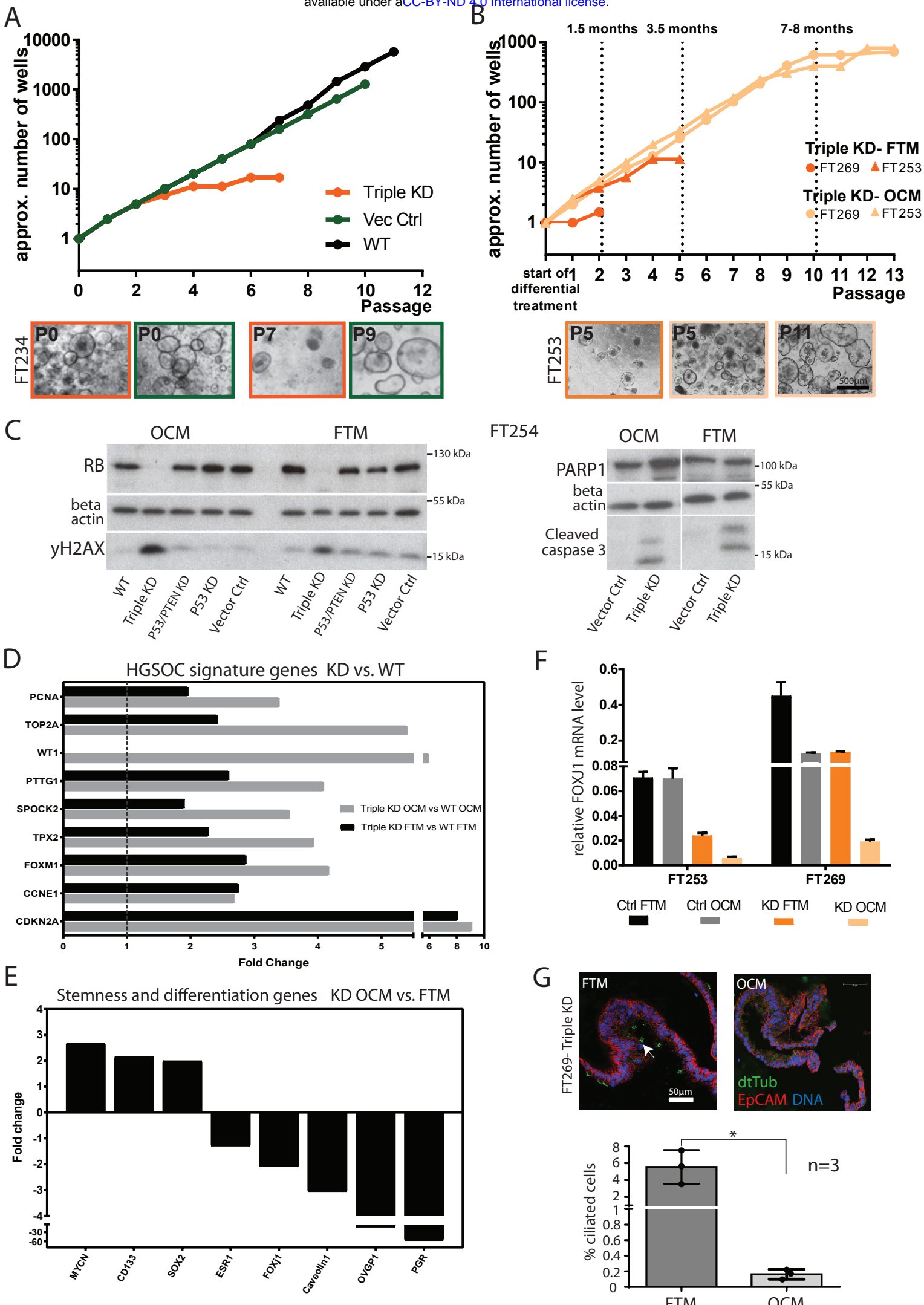


## Figure 5. Wnt deprivation supports preservation of stemness in HGSC organoids.

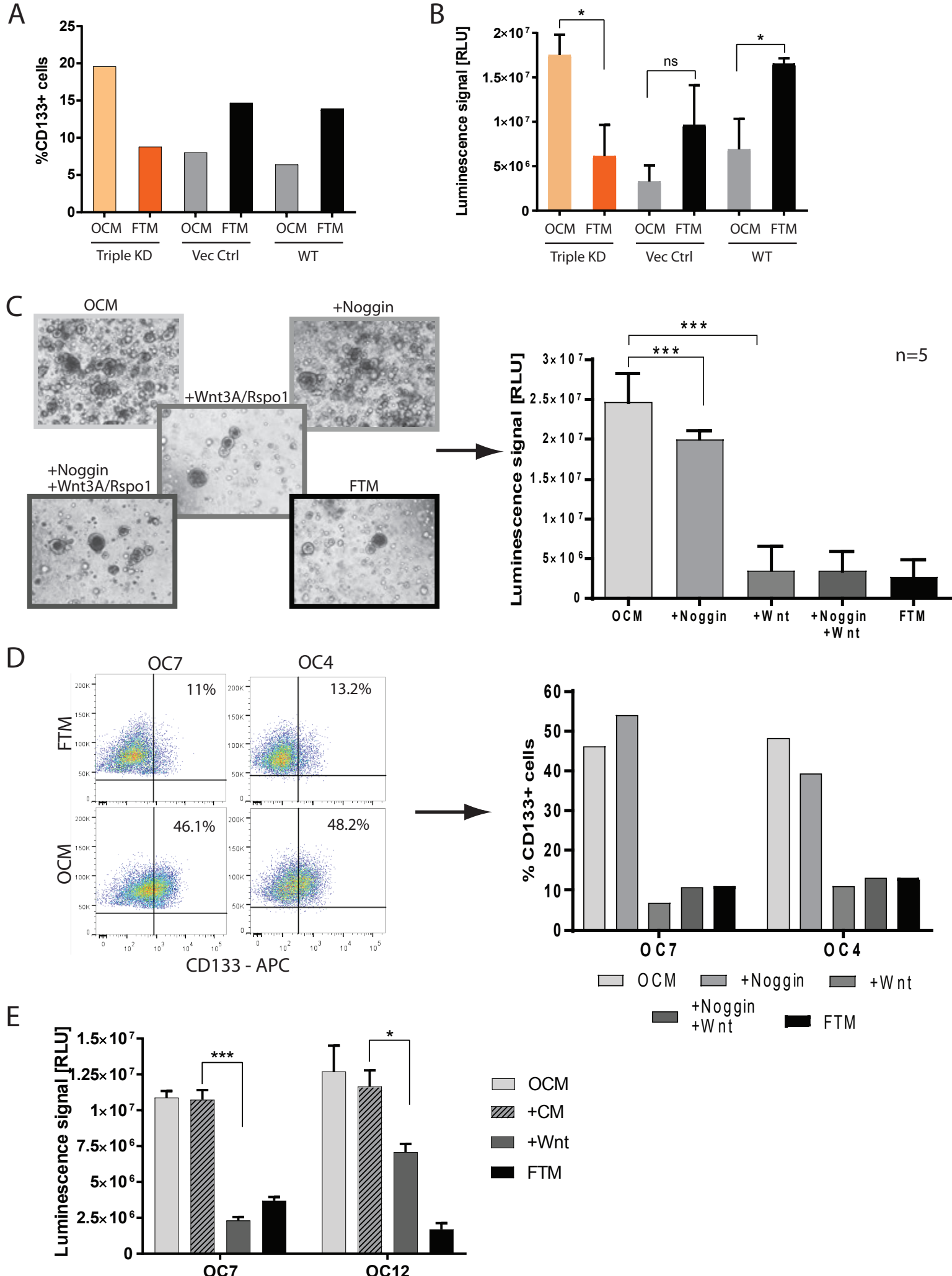
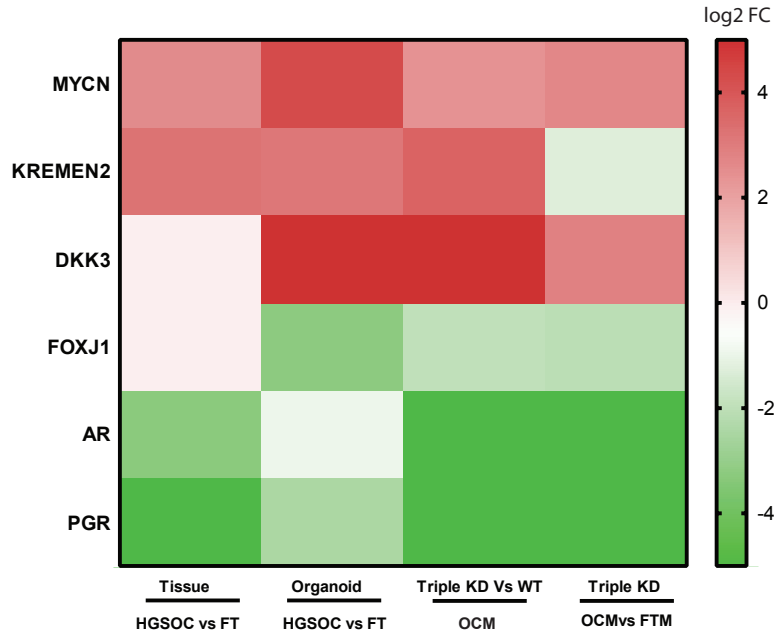
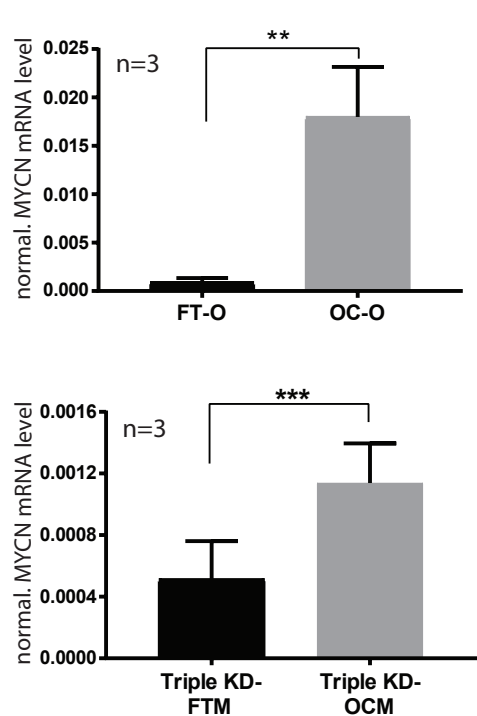


## Figure 6. Unifying induction of MYCN and its inhibitors in HGSOC and KD samples.

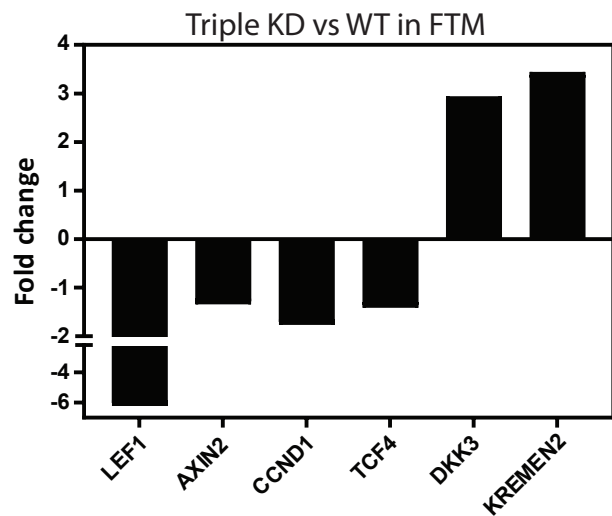
A



B



C



D

